1990-12

The design of a new far ultraviolet interferometer for ionospheric spectroscopy

Nichols, James Warren

Monterey, California: Naval Postgraduate School

NAVAL POSTGRADUATE SCHOOL
Monterey, California

THESIS

THE DESIGN OF A NEW FAR ULTRAVIOLET INTERFEROMETER FOR IONOSPHERIC SPECTROSCOPY

by

James Warren Nichols

DECEMBER 1990

Thesis Advisor: David D. Cleary
Co-Advisor: D. Scott Davis

Approved for public release: Distribution is unlimited

SECURITY CLASSIFICATION OF THIS PAGE

REPORT DOCUMENTATION PAGE

Form Approved OMB No 0704-0188

1a REPORT SECURITY CLASSIFICATION: Unclassified	1b RESTRICTIVE MARKINGS
2a SECURITY CLASSIFICATION AUTHORITY	3 DISTRIBUTION / AVAILABILITY OF REPORT: Approved for public release: Distribution is unlimited
2b DECLASSIFICATION / DOWNGRADING SCHEDULE	
4 PERFORMING ORGANIZATION REPORT NUMBER(S)	5 MONITORING ORGANIZATION REPORT NUMBER(S)
6a NAME OF PERFORMING ORGANIZATION: Naval Postgraduate School; 6b OFFICE SYMBOL (If applicable): PH	7a NAME OF MONITORING ORGANIZATION: Naval Postgraduate School
6c ADDRESS (City, State, and ZIP Code): Monterey, CA 93943-5000	7b ADDRESS (City, State and ZIP Code): Monterey, CA 93943-5000
8a NAME OF FUNDING / SPONSORING ORGANIZATION; 8b OFFICE SYMBOL (If applicable)	9 PROCUREMENT INSTRUMENT IDENTIFICATION NUMBER
8c ADDRESS (City, State, and ZIP Code)	10 SOURCE OF FUNDING NUMBERS: PROGRAM ELEMENT NO; PROJECT NO; TASK NO; WORK UNIT ACCESSION NO

11 TITLE (Include Security Classification)
THE DESIGN OF A NEW FAR ULTRAVIOLET INTERFEROMETER FOR IONOSPHERIC SPECTROSCOPY

12 PERSONAL AUTHOR(S)
JAMES WARREN NICHOLS

13a TYPE OF REPORT	13b TIME COVERED	14 DATE OF REPORT (Year, Month, Day)	15 PAGE COUNT
Master's Thesis	FROM _____ TO _____	DECEMBER 1990	77

16 SUPPLEMENTARY NOTATION
The views expressed in this thesis are those of the author and do not reflect the official policy or position of the Department of Defense or the U.S. Government

17 COSATI CODES		
FIELD	GROUP	SUB-GROUP

18 SUBJECT TERMS (Continue on reverse if necessary and identify by block number)
Ionosphere, Ultraviolet spectroscopy, interferometer

19 ABSTRACT (Continue on reverse if necessary and identify by block number)

A new far ultraviolet interferometer for ionospheric spectroscopy was designed and tested. The design uses a concave spherical grating in an off-plane Rowland circle configuration. Wave fronts are split into zero and negative first order diffractions, reflected by plane mirrors and recombined by the spherical grating to produce interference fringes. Use of a single concave grating reduces the total number of reflections to three for each path. The off-plane configuration was required to obtain equal path lengths. The ruling density was selected to eliminate other diffracted orders. The design was tested first by verifying the feasibilty of recombining a divided wave front using two similar flat transmission gratings. Next a concave grating interferometer using a helium neon laser as the source. The design produced a high quality fringe pattern suitable for spectroscopic analysis.

20 DISTRIBUTION AVAILABILITY OF ABSTRACT	21 ABSTRACT SECURITY CLASSIFICATION
☒ UNCLASSIFIED/UNLIMITED ☐ SAME AS RPT ☐ DTIC USERS	unclassified

22a NAME OF RESPONSIBLE INDIVIDUAL	22b TELEPHONE (Include Area Code)	22c OFFICE SYMBOL
David D. Cleary	(408) 646-2382	PH

DD Form 1473, JUN [redacted] Obsolete

SECURITY CLASSIFICATION OF THIS PAGE

4-6603

UNCLASSIFIED

Approved for public release: Distribution is unlimited

The Design of a New Far Ultraviolet Interferometer
for Ionospheric Spectroscopy

by

James Warren Nichols
Major, United States Army
B.S., United States Military Academy, 1978

Submitted in partial fulfillment of the
requirements for the degree of

MASTER OF SCIENCE
IN PHYSICS

from the

NAVAL POSTGRADUATE SCHOOL

DECEMBER 1990

Author: [redacted]

James Warren Nichols

Approved by: [redacted]

David D. Cleary, Thesis Advisor

[redacted]

D. Scott Davis, Co-Advisor

[redacted]

Karlheinz Edgar Woehler, Chairman
Department of Physics

ABSTRACT

A new far ultraviolet interferometer for ionospheric spectroscopy was designed and tested. The design uses a concave spherical grating in an off-plane Rowland circle contiguration. Wave fronts are split into zero and negative first order diffractions, reflected by plane mirrors and recombined by the spherical grating to produce interference fringes. Use of a single concave grating reduces the total number of reflections to three for each path. The off-plane configuration was required to obtain equal path lengths. The ruling density was selected to eliminate other diffracted orders. The design was tested first by verifying the feasibilty of recombining a divided wave front using two similar flat transmission gratings. Next a concave grating interferometer was built and tested using a helium neon laser as the source. The design produced a high quality fringe pattern suitable for spectroscopic analysis.

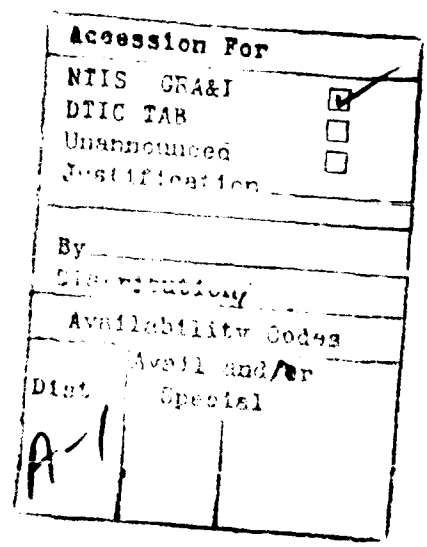

TABLE OF CONTENTS

LIST OF FIGURES

LIST OF TABLES

I. INTRODUCTION

The variation of electron density in the earth's ionosphere is a subject of immediate value for military applications as well as general scientific interest. The Naval Postgraduate School has been involved in that study most recently with the flight of the Mustang experiment in March of 1990 (Clayton, 1990; Andersen, 1990). Mustang is a middle ultraviolet spectrometer for observation of emissions between 1800 Å and 3400 Å in the E, F1, and F2 regions of the earth's ionosphere. The ability to model electron density from spectral analysis of ions is the focus of the research. A high resolution spectrometer for ionospheric investigation is needed to complement the capabilities of other lower resolution, but broader spectral passband instruments like Mustang.

A. THESIS GOALS

The goal of this thesis is to design an interferometer capable of high resolution far ultraviolet spectroscopy in a space environment. The design is to be tested in the laboratory and verified for feasibility. Visible light will be used in the laboratory as the source for testing. The design must improve on previous designs by increasing sensitivity, yet remain capable of flying on sounding rocket experiments.

B. THESIS OUTLINE

Chapter II of the thesis provides the background and motivation for the thesis. It gives a basic picture of the ionosphere, its importance to military systems, and a brief summary of previous research. Chapter III contains theory important to the design of an interferometer, including sections on interference, diffraction, and spherical gratings. Chapter IV contains two sections. The first deals with a preliminary laboratory experiment using a two grating interferometer to test the principle of recombining diffracted wave fronts. The second covers the process followed in designing the actual instrument. Chapter V presents the results of testing the design, and Chapter VI presents conclusions and recommendations for further development.

II. BACKGROUND

A. THE IONOSPHERE

Understanding the nature and processes of the earth's ionosphere is essential for appreciation of the importance of measuring the ionosphere for different military and civilian applications. The ionosphere is so named because it is the primary region for photoionization of atoms and molecules by solar radiation. The plasma of the ionosphere is the reflective medium which allows over-the-horizon (OTH) transmission of electromagnetic signals.

The regions of the earth's atmosphere are divided into horizontal layers due to the different densities and physical characteristics of the constituents. The temperature profile as a function of altitude is shown in Figure 2.1. As one would expect, the temperature drops off gradually with altitude in the troposphere, the region closest to the earth's surface. It drops off at a fairly constant rate of about 7 K/km up to about ten kilometers where the temperature begins to rise. This first inflection point for the temperature curve is called the tropopause. The tropopause defines the boundary between the troposphere, where conductive energy transport is important, and the stratosphere where the atmosphere is warmed by direct absorption of solar radiation. This absorption causes the temperature profile of the stratosphere to increase with altitude, since higher regions experience the greater fluxes of incoming radiation. At about 50 km there is another inflection point in the

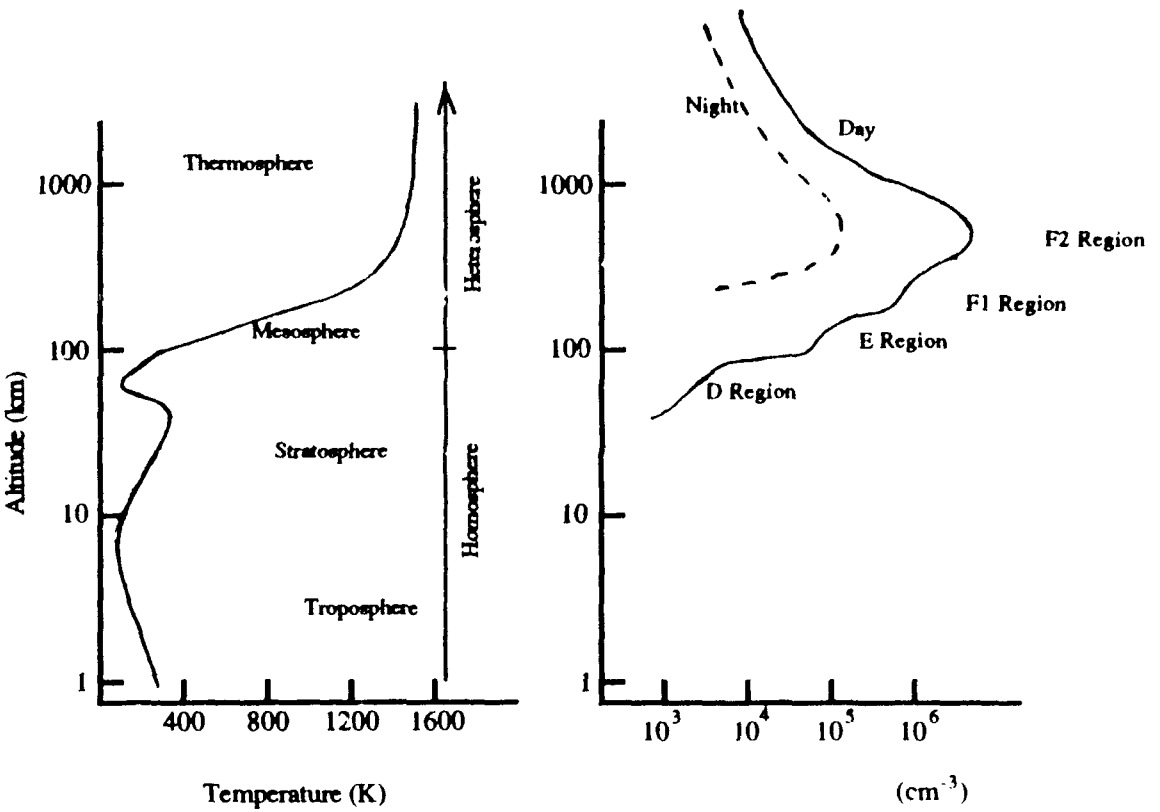

Figure 2.1. Regions of the Atmosphere and Ionosphere.

profile called the stratopause. Here, the radiative heat loss is greater than the absorption, and there is a rapid decrease in temperature with altitude until the mesopause is reached at about 80 km. This region of rapidly decreasing temperature is the mesosphere. Above the mesopause the temperature rises dramatically, reaching values above 1000 K. This rapid rise in temperature is caused by the absorption of another portion of the ultraviolet solar radiation. This upper altitude high temperature region is called the thermosphere.

The earth's atmospheric layers are also defined by the nature of their constituents. Below about 100 km, the atmosphere undergoes a great deal of mixing due to temperature gradients and resulting convection. This is referred to as the homosphere because of the even mixture of the component gases. At 100 km altitude, the mean free path for a particle is about 300 meters. Collisions and mixing are much less likely. In this region the different gases are separated into layers according to their densities. This is the heterosphere.

The ionosphere is defined as that part of the earth's atmosphere having sufficient density of charged particles to affect the propagation of electromagnetic energy. Generally speaking, this extends from an altitude of about 50 km outward to the furthest extent of the earth's atmosphere. The ionosphere is divided into D, E, and F regions. The chemistry that produces ions, and therefore the charged particle density in each region is different. The E region was discovered first and so named because it was a region of high electron density. The D and F regions were discovered later and named to coincide with their position relative to the E region.

The ions and electrons are not the primary particles in the ionosphere. In fact, their density may be less than 1/1000th of the density of the neutral atoms and molecules. Additionally, since the electrons are the result of the ionization of atoms or molecules, the net charge of the ionosphere is neutral. However, free charges are present, and these are responsible for the electromagnetic properties of the ionosphere. Since solar radiation is the energy source for photoionization, the ion density varies with the earth's daily rotation, solar flares, and solar cycles.

The D region is the lowest layer of the ionosphere, located between 50 and 90 km altitude. Since it is the lowest region, the radiation that affects it must have penetrated through a considerable depth of atmosphere, and consequently the ion density is small compared to the other regions. The maximum concentration of ions is between 75 and 80 km. Ionization is primarily caused by absorption of the Lyman α solar line by NO, although during periods of solar flares hard x-ray ionization of molecular oxygen and nitrogen can reach the same magnitude. Ion densities in the D region peak at about 10^4 cm^{-3} in the daytime. At night the densities in the lower latitudes drop to near zero. Since the D region is at a fairly low altitude, atmospheric density is high, and therefore the rate of recombination is also high. At night it is much greater than the rate of ionization. At latitudes greater than 60° the ion densities do not drop off as rapidly at night. Here, interactions with charged particles trapped in the earth's magnetic field sustain the ionization rate.

The E region of the ionosphere lies between 90 and 140 km altitude. The primary source of ionization is absorption of extreme ultraviolet and soft x-rays by O_2

and atomic oxygen. The atomic oxygen process dominates near the top of the region. Ionized O_2 transfers its charge to NO molecules, so that the principal ions (in order of density) are NO^+, O_2^+, and O^+. The E region also disappears at night, except at higher latitudes. During the day the peak density can reach 10^5 cm^{-3} at an altitude of 100 km.

The F1 region is a narrow region that is like a shelf of intermediate density between the F2 region and the E region. Ionization is due primarily to the absorption of extreme ultraviolet radiation by atomic oxygen. The F1 region is located from about 140 to 200 km altitude and is therefore part of the heterosphere. This means that the lighter particles will exist in the higher layers and receive the largest flux of incident radiation. Additionally, because of the separation of constituents, charge transfer does not occur, and O^+ is the primary ion. The F1 region also disappears at night. Maximum ion densities on the order of 3×10^5 cm^{-3} are reached during summer months and periods of increased solar activity.

The F2 region occurs above 200 km. It does not disappear at night because of the low rate of electron-ion recombination, because the atmospheric density is too low at this altitude for sufficient particle collisions. Again, the major ion is O^+ produced by the absorption of radiation below 800 Å. The electron density is greatest during the daylight hours as expected, but seasonally is greatest in the winter. This is known as the winter anomaly and is caused by thermospheric winds which transport electrons from the summer hemisphere to the winter hemisphere. The

height of the greatest electron density varies greatly with the hour of the day, season, and level of solar activity.

B. MOTIVATION FOR STUDY

The ionosphere is a conducting medium and as such has a significant impact on the propagation of electromagnetic energy. In terms of pure scientific research, this means that signals to and from all types of orbiting satellites, electronic space probes, and communications reflected from the ionosphere undergo a certain amount of distortion. Specifically, the radio frequency pulse shape can be dispersed by electron density irregularities. For this reason, a great deal of research aimed at understanding these distortions has been done, with the goal of developing means to correct for them.

Models of the ionosphere's charge density have been developed from data collected over many years, both from land based radio wave probes and from rocket borne experiments. The "International Reference Ionosphere" is now the internationally preferred model. It maps critical frequencies measured by ionosondes around the world. Median values are obtained for each 24 hour day and different ranges of solar activity. The model is limited in that the daily variance can be as much as 25%, and solar activity can only be modeled up to a certain value. Additionally, the ionosonde is a land based system, and so large extrapolation of the data must be done to expand the model over the earth's surface. Also, forecasters have some difficulty in predicting details of the solar cycle. Despite these limitations,

the model is a significant factor in reducing error in a number of systems. For example, range errors in satellite tracking are reduced as much as 75%. However, a system for continuously monitoring the profile of the ionosphere over large portions of the earth's surface has yet to be developed.

The extensive military use of satellite communications, navigation, and observation systems makes modeling and monitoring the ionosphere extremely important. Additionally, some long range communications systems depend on ionospheric reflection of the radio frequency signal. OTH radar is an example of a new technology that will require real-time data on ionospheric conditions to operate effectively. The military requirement for charge density profiles of the ionosphere has provided much of the impetus for ionospheric research.

C. HISTORY OF RESEARCH

The Naval Research Laboratory (NRL) has worked for a number of years on measuring the ionosphere through remote sensing of ultraviolet emissions (Anderson et al., 1976). The electron density is tied to the ion density, which can be derived from measurements of each ion's spectral emissions. A system of monitoring satellites, much like those used in meteorology, is envisioned to provide real-time data over all desired regions of the earth's surface.

As a step toward that goal, NRL and the Naval Postgraduate School flew two complementary experiments on a NASA sounding rocket at White Sands Missile Range in March, 1990. The High Resolution Airglow and Aurora Spectrograph

(HIRAAS) is a 0.5 m Rowland spectrograph with an electrographic camera detector. It was designed to observe emissions from 500 to 1500 Å, including the O^+ 834 Å triplet. Attached to the HIRAAS for flight was the NPS Middle Ultraviolet Spectrometer (MUSTANG). MUSTANG was designed to look at emissions from 1800 to 3400 Å, specifically those from nitrogen gases. MUSTANG produced over 6000 spectra during the 14 minute flight. These spectra were averaged into ten km altitude bins for data analysis. (Clayton, 1990; Andersen, 1990)

Both HIRAAS and MUSTANG observed a broad wavelength band to examine several emission lines. This capability can provide new information that will improve modeling of the ionosphere by linking emissions to ion density. To further understand the processes affecting individual ions, a higher resolution spectrometer that examines the profile of a single spectral line is required.

III. THEORY

A. INTERFERENCE

Measurements of ultraviolet spectra of the ionosphere are performed using interference spectroscopic methods, such as diffraction gratings. Simple dispersive instruments based on prism technology won't work, because no window materials transmit radiation below 1040 Å. Therefore, interference spectroscopy, using all-reflecting optics, is necessary. Interference caused by overlapping wave fronts is well understood. Interferometers have been developed for applications in industry as well as science. The theory behind transmission devices and reflection devices is the same. The discussion which follows is found in many texts on optics, including those by Jenkins and White (1976) and Hecht (1988).

Explaining interference requires use of the wave theory for the electromagnetic nature of light as opposed to the particle or corpuscular model. When two wave fronts intersect, there is an interaction between the two in the region of overlap. This interaction cannot be explained simply by summing the intensity of the two beams. Using wave theory, however, it is possible to correctly predict the optical disturbance. The equations describing the wave fronts obey the principle of superposition, and so the net electromagnetic field is the vector sum for the two waves' individual fields.

When examining interference, irradiance is the property generally measured. Irradiance is proportional to the time average of the square of the amplitude of the incident electric field. The constant of proportionality is a function of the medium, and, since the experiment deals with media whose refractive indices are

approximately unity, it will be ignored here. In overlapping wave fronts, the electric field is the vector sum of the two fields for each front or

$$\vec{E}_t = \vec{E}_1 + \vec{E}_2 \quad .$$

The irradiance then is defined by

$$I = \langle \vec{E}_t^2 \rangle$$

where $\langle\ \rangle$ is the time average and

$$\vec{E}_t^2 = \vec{E}_t \cdot \vec{E}_t = (\vec{E}_1 + \vec{E}_2) \cdot (\vec{E}_1 + \vec{E}_2)$$

or

$$\vec{E}_t^2 = \vec{E}_1^2 + \vec{E}_2^2 + 2\vec{E}_1 \cdot \vec{E}_2 \quad .$$

The total irradiance can then be expressed as

$$I = I_1 + I_2 + I_{12}$$

if I_1, I_2, and I_{12} are defined as

$$I_1 = \langle \vec{E}_1^2 \rangle \quad , \quad I_2 = \langle \vec{E}_2^2 \rangle \quad , \quad \text{and} \quad I_{12} = 2\langle \vec{E}_1 \cdot \vec{E}_2 \rangle \quad .$$

The last term is the interference term. The electric field intensity for a plane harmonic electromagnetic wave is expressed generally as

$$\vec{E}(\vec{r},t) = \vec{E}_0 \cos(\vec{k} \cdot \vec{r} - \omega t + \varepsilon)$$

where E_0 is the amplitude vector, $\vec{k}$ is the wave vector, $\vec{r}$ is the position vector, ωt represents the phase of the wave as a function of frequency and time, and ε is an

initial phase shift. If the interference involves the overlapping of two such waves of the same frequency then

$$I_{12} = \vec{E}_{0_1} \cdot \vec{E}_{0_2} \cos\delta$$

where

$$\delta = (\vec{k}_1 \cdot \vec{r} - \vec{k}_2 \cdot \vec{r} + \varepsilon_1 - \varepsilon_2) \quad .$$

If the two wave fronts propagate so that their electric field vectors are parallel, the dot product reduces to the scalar multiplication of the two amplitudes and

$$I_{12} = E_{0_1} E_{0_2} \cos\delta \quad .$$

Additionally, since the average value of the cosine function squared is ½, the irradiance can be expressed as

$$I = \langle \vec{E}^2 \rangle = \frac{E_0^2}{2} \quad .$$

This simplifies the expression for the irradiance of the overlapping wave fronts to

$$I = I_1 + I_2 + 2\sqrt{I_1 I_2} \cos\delta \quad .$$

Maxima occur when δ is equal to zero and even integer multiples of π, minima for odd integer multiples. Wave fronts of the same frequency and propagating in parallel directions produce a fringe pattern dependent only on the difference in phase between two wave fronts. Additionally, as the angle between overlapping wave fronts increases, the fringes get closer together.

For interference fringe patterns to be measurable, an important relationship between the wave fronts' sources must exist. The two sources need not be in phase

with one another, but the relationship between their phases must be constant during the measurement. Such sources are said to be coherent. Because of this, many interferometers rely on a single source in which the wave front is divided into two paths, thereby creating two coherent virtual sources from a real source. Radiation from a single source is not an infinite harmonic wave chain. The light propagates in wave groups, within which the electric field intensity is described by a narrow distribution of sinusoidal wave functions. However, these wave groups are relatively short: the length of a group is proportional to the group's frequency distribution. Since each wave group is so short, if two independent sources are used, the wave groups will not be correlated stably during the observation time, and the fringe pattern would change so rapidly as to be indiscernible.

Exceptions to the rule for single source experiments use lasers and microwave radiation to produce interference fringes. These sources have extremely long coherence lengths, corresponding to very narrow group frequency distributions. The coherence length for a particular wavelength of a given source is a function of the natural width of the spectral line and the physical environment of the source. The wave trains formed by the emitting atoms of the source have their frequency altered by thermal motions and electric and magnetic fields. These effects can widen each spectral line, giving it a frequency bandwidth

$$\Delta\nu \sim \frac{1}{\Delta t_c}$$

where Δt_c is the coherence time. The coherence length is just the length of each wave group. The coherence time is the duration of time for the passage of a wave group. So,

$$\Delta x_c = c\Delta t_c \quad .$$

The width of a spectral line, or the width in its frequency distribution, is therefore a measure of its coherence length. The coherence length is not necessarily constant. It changes as the external factors already mentioned change the breadth of the line, eg., thermal Doppler broadening. Spectral lines from standard laboratory source lamps have coherence lengths on the order of a few millimeters, while those for infrared lasers can be several kilometers. Since the ability to discern fringe patterns depends on the correlation of the overlapping wave fronts, it is obviously a much easier task to obtain stable fringe patterns from a laser source than from a laboratory lamp.

Interferometers have traditionally been divided into two categories, wave front splitting and amplitude splitting. Wave front splitting interferometers divide each wave front of the incident radiation to produce interference, usually through diffraction from multiple slits, as with transmission gratings. Amplitude splitting interferometers do not affect the continuity of each wave front but divide the amplitude of the electromagnetic field vectors, sending separate wave trains along two or more distinct paths. This is usually accomplished through the use of partially reflecting surfaces called beam splitters. The Michelson interferometer is an example. The design to be used in this experiment is a hybrid. It uses wave front splitting optics, but it has a great deal of similarity to many amplitude splitting interferometers in terms of geometry.

Interferometers play an important role in spectroscopy. The Fabry-Perot interferometer is used to examine the fine structure of individual spectral lines. Interference spectrometers are especially advantageous for faint sources because of

Interference spectrometers are especially advantageous for faint sources because of their greater sensitivity and small size for high resolution. (Roesler, 1974 and Harlander et al., 1990). In these spectrometers, Fourier analysis of fringe patterns produces the desired spectra. Interferometers for spectroscopy are especially well suited for analysis of the infrared region of the electromagnetic spectrum.

B. DIFFRACTION

Diffraction is the bending of a wave front when it encounters an obstruction. As with interference, it is most easily analyzed using wave theory. Geometric optics can also be used in a quantum approach. The explanation of diffraction begins with Huygens principle of secondary wavelets. Interference between these secondary wave fronts is the cause of diffraction. In this way, diffraction and interference are closely related physical phenomenon. Fresnel, or near-field diffraction, occurs when the plane of observation is close to the obstruction. Here the image of the obstruction is plainly visible but has fringes around the edges. Fraunhofer, or far-field diffraction, occurs when the plane of observation is far from the obstruction so that the diffraction pattern and not the object itself is observed. Fraunhofer diffraction is commonly used for spectroscopy and is discussed here.

Diffraction of a plane-parallel monochromatic wave front by many slits, or a grating is illustrated in Figure 3.1. Diffraction patterns are produced by each of the spherical wave fronts exiting the slits as they arrive at a given point on the observation plane. Constructive interference of the spherical wave fronts can be observed along several directions of propagation, when all wave fronts interfere in phase with one another. These correspond to the different orders of diffraction for the wave front. The grating equation is

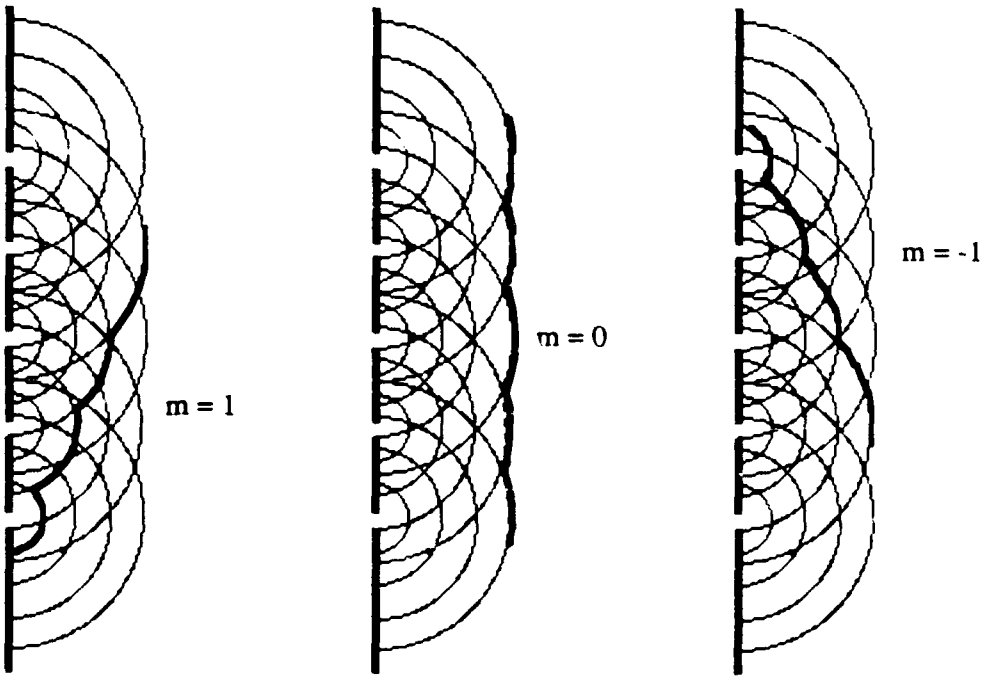

Figure 3.1. Diffraction from Multiple Slits.

$$m\lambda = a \sin\theta$$

where a is the spacing between the center of each aperture, λ is the wavelength, m is the diffraction order, and θ is the angle the direction of propagation makes with the grating normal.

For transmission gratings, a difference in optical path lengths is created by variation is the thickness of the grating in the rulings or by obscurations. For reflection gratings the difference in path length comes typically from the different depth of travel to the surface of the grating for reflection or from different orientations of regions of the grating surface. Additionally the incident wave front need not be parallel to the grating normal (see Figure 3.2). If it is not, the grating equation becomes

$$d(\sin\theta_m + \sin\theta_i) = m\lambda \quad , \tag{3.1}$$

where θ_m is the angle of reflection for the m^{th} order diffraction and θ_i is the incident angle of radiation. Both are measured positive clockwise from the grating normal. This is the most general form for the grating equation in two dimensions.

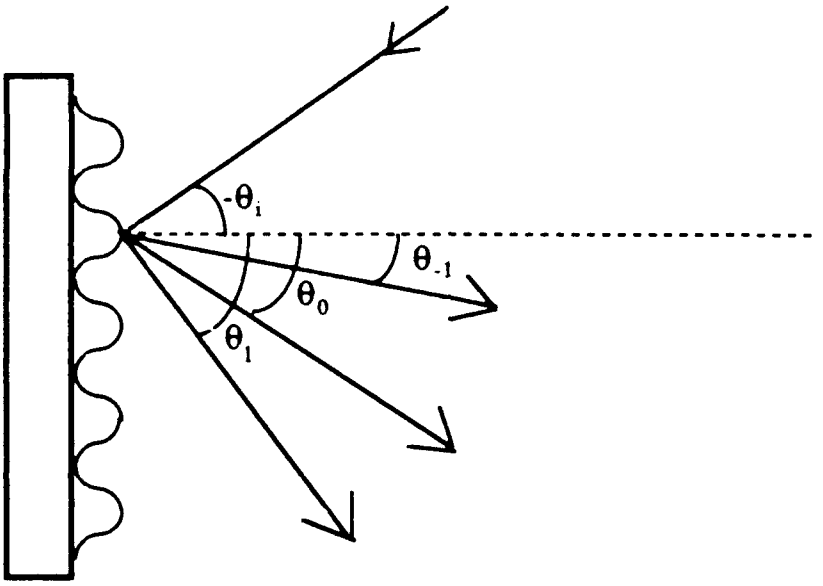

Figure 3.2. Diffraction of Non-Normal Radiation.

C. SPHERICAL GRATINGS

In 1882 H.A. Rowland published his design for a vacuum spectrometer using the characteristics of both diffraction gratings and spherical mirrors. Rowland found that a spherical concave reflective grating had the property that any image emanating from a point on a circle of diameter equal to the radius of the grating and tangent to its surface would be diffracted and focused at some point on the circumference of the same circle. The Rowland circle mount is depicted in Figure 3.3.

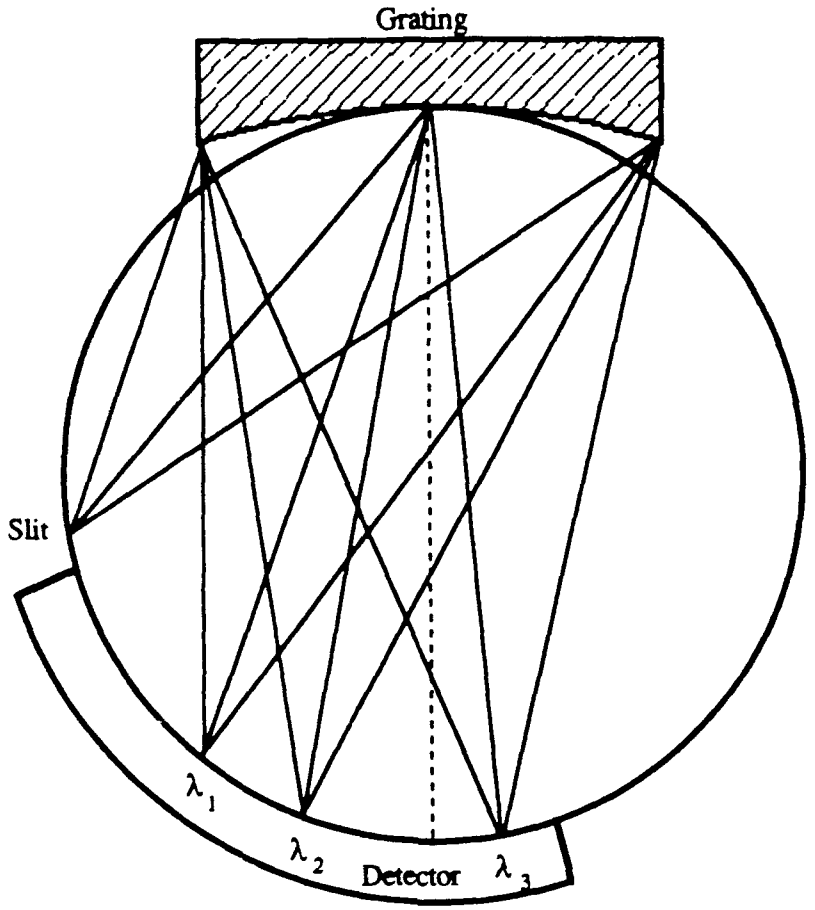

Figure 3.3. Rowland Circle Mount.

Generally speaking, Rowland circle spectrometers are used for broad wavelength coverage and have slit and focal points on the plane containing the grating normal. Usually, the Rowland circle is perpendicular to the grating rulings. However, some spectrometers adopted an off-plane or Eagle mount for cases where the angle of incidence and the diffraction angle were about equal and vertical separations allowed physical positioning of the slit and detector plate at or near the same horizontal angle. These spectrometers have been shown not to suffer significantly in resolution (Namioka, 1959) if the angular deviation of the slit and

plate is small. However, a modification is required to the general grating equation for the off-plane deviation. That is

$$\frac{m\lambda}{a} = \left(1 + \frac{z_0^2}{R^2 \cos^2\theta_i}\right)^{-\frac{1}{2}} (\sin\theta_m + \sin\theta_i) \qquad (3.2)$$

where z_0 is the vertical offset of the slit above the plane, and R is the radius of the grating. Given a particular detector, source, and grating, z_0, λ, and a are fixed. This implies that the instrument should be large since increasing R is the only way to reduce the impact of the offset. The design proposed in this thesis, however, does not rely on the resolution of a single spectral line but the interference fringes of two divided wave fronts. Therefore, although minimizing deviation angles above the plane is desirable to improve imaging, it is not as critical to the resolution of the instrument.

Astigmatism associated with a spherical mirror, however, remains a concern. For spherical concave mirrors, a point source off the axis of the mirror is imaged as two mutually perpendicular lines offset spatially from one another. One line is formed in the tangential plane as the primary image and the other in the sagittal plane as the secondary. If the source lies on the axis of the mirror, the two planes intersect and a stigmatic point image is produced. The incident and reflected beams describe the tangential plane. The tangential plane for a Rowland circle mount would place a vertical image of a point source on the circumference of the Rowland circle. The secondary image would be a horizontal line in the plane perpendicular to the grating axis and tangent to the circumference. (See Figure 3.4.) For an off-axis mount, these images would no longer be horizontal and vertical in relation to the Rowland circle

plane, but instead with a coordinate system rotated in space by the same angle between the center ray from the image to the grating and the grating normal.

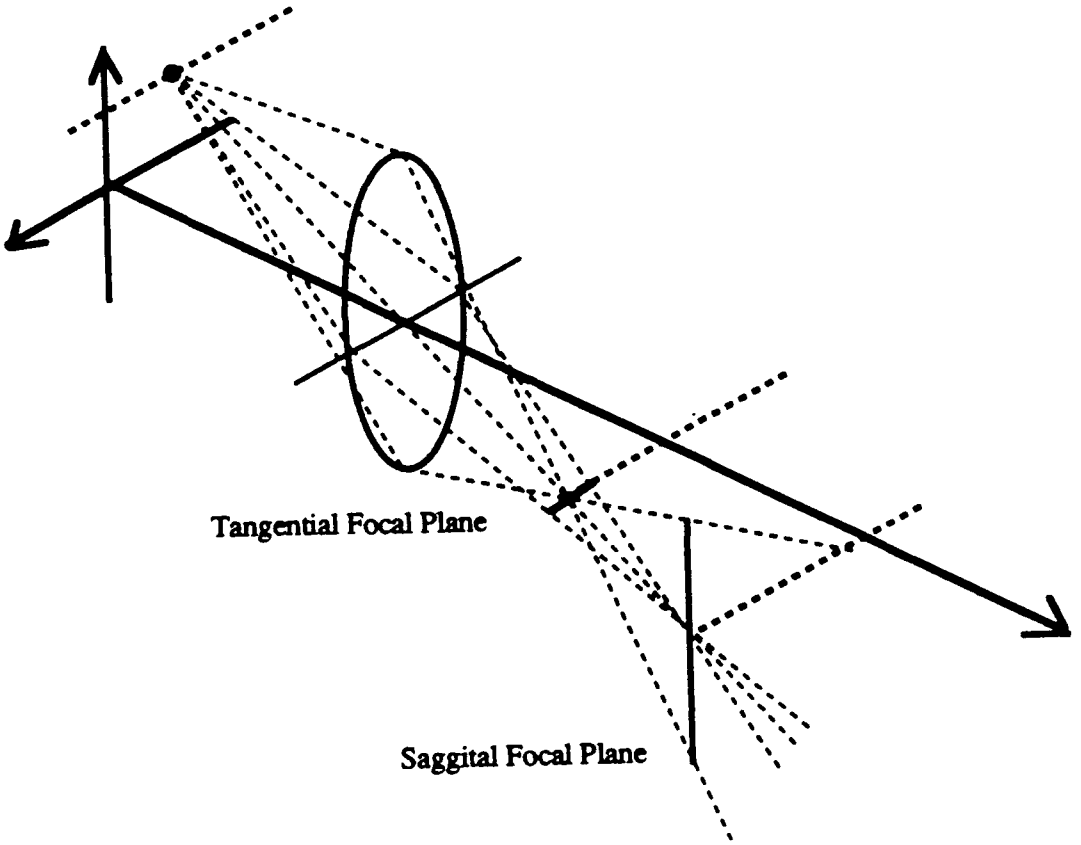

Figure 3.4. Astigamtism.

IV. EXPERIMENTAL PROCEDURE

A. TWO GRATING INTERFEROMETER

The first step in the experimental procedure was to verify that a wave front could be split into two paths and then recombined to produce an interference pattern using two transmission gratings. The final instrument was to be designed for use in the far ultraviolet region. This meant that all devices used for controlling the path of the electromagnetic radiation would have to be reflective surfaces, since no material exists capable of transmitting radiation of wavelengths shorter than 1040 Å. (See e.g., Samson, 1967.) However, visible light was selected for initial testing of the concept because of the obvious simplification this made to aligning the optical devices to split, reflect, and recombine the wave front and to detect the result. Therefore, it was possible to use transmission gratings for initial testing while the reflection grating required for final proof of concept was being manufactured.

The layout of the equipment used in this first trial is depicted in Figure 4.1. In this setup light emitted by the source is passed through a narrow slit to represent a one dimensional source. A collimating lens is used to produce a plane parallel wave front. The first grating diffracts the transmitted light by wavelength according to the grating equation (See Equation 3.1) into different angles. The zero order light passing directly through the grating is blocked by a baffle called the zero order absorber (ZOA). Plane mirrors are placed at appropriate locations parallel to the original path

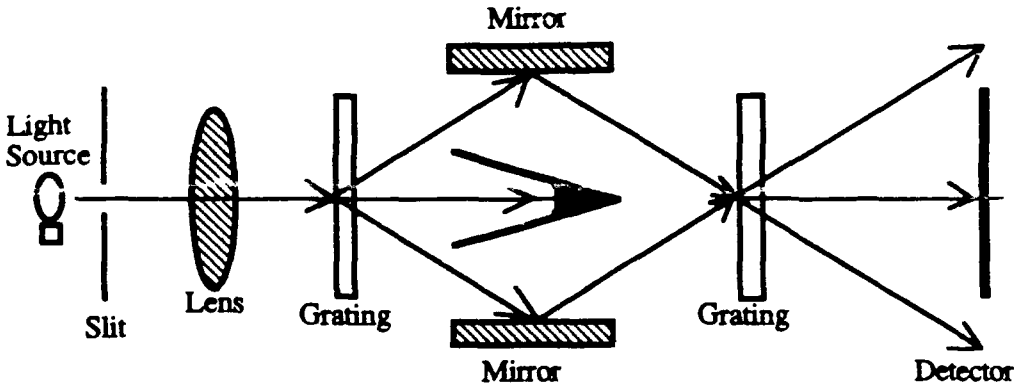

Figure 4.1. Two Grating Interferometer.

of the collimated beam to reflect only the positive and negative first orders of diffracted light. The ZOA serves a second purpose by blocking any reflection between the two mirrors. The reflected light is then recombined onto nearly coincident paths on passing through the second grating. If the optical path lengths of the two paths and the ruling density of both gratings are exactly the same, the two wave fronts should coincide exactly in phase and direction on recombination and only a uniform intensity plane wave front would appear. Since perfect alignment of the system is not possible, the recombined beams will be slightly out of phase and the wave fronts not perfectly parallel. The overlapping, nonparallel wave fronts produce an interference pattern if the difference in phase is smaller than the coherence length of the particular spectral line selected by placement of the mirrors.

Selection of equipment was based on the spectral properties of the initial source, a 65 watt sodium arc lamp. Sodium was chosen as the source because of the easily distinguishable doublet at 5896 and 5890 Å. Grating ruling densities were desired so

that the first order diffractions would be at angles greater than 20 degrees. Larger angles would require more accuracy in mirror placement to obtain equal path lengths. Gratings with reported densities of 25,000 and 25,100 lines per inch were available. Although exactly equal densities were preferable, these were within one percent and deemed acceptable. A CCD video camera without lens was to be used as the detector. The lens used for collimation had a focal length of 10.7 centimeters. This was used because the focal length was a good compromise between separating equipment and minimizing the overall length of the apparatus.

Alignment of the apparatus was carried out using simple optical procedures. The source was placed in a light-tight box with a circular aperture opening toward the slit. The slit and aperture were placed at the same height using a height gauge. The lens was placed on the same line on the optical table as the slit, and again height was verified with the gauge. Horizontal distance from slit to lens was established using a telescope adjusted for focus at infinity. The lens was slid along the optical table on the horizontal axis of the apparatus until the slit image was focused in the telescope. This effectively collimated the image leaving the lens. The grating was placed a nominal distance from the lens at the same height. The grating rulings were made vertical by insuring that the negative and positive order diffractions were at the same height as the zero order. Mirrors were placed two rails (12.6 cm) out from the horizontal axis on the optical table. The mirrors were adjusted to the same height and adjusted so that their faces were parallel to the vertical axis. Adjustment of the mirrors about horizontal and vertical axes of rotation was accomplished by

placing a target at the calculated location for the second grating. The mirrors were canted about these axes until the image from the positive and negative first order diffractions overlapped that of the zero order. Next the target was replaced by the second grating. Its rulings were verified to be vertical in the same manner as the first. Finally the ZOA was placed between the mirrors, and the camera was placed at the end of the apparatus. Its actual horizontal distance from the second grating was not a critical dimension. Since the slit image was collimated, an interference pattern would be observable at any distance beyond the second grating where sufficient intensity remained. However, it did need to be placed far enough away from the second grating so that the images from the mirrors which passed directly through the second grating (zero order) did not enter the aperture of the camera. Dimensions of the final setup are shown in Figure 4.2.

First tests of this apparatus showed that the CCD camera was not sensitive enough to detect the slit image after two diffractions where the zero order was eliminated. The camera was replaced with a photographic plate so that long exposure photographs of the image could be taken. Polaroid 57 film, ISO 3000 was used. Exposures between five and ten minutes were tried. The vertical slit image observed could be seen to be the overlap of two single images. There was only a slight offset initially between the two. Vertical lines appeared in the slit image. At first these were believed to be the interference fringes that were sought. However, when one arm of the interferometer was blocked, the vertical lines remained and therefore could not

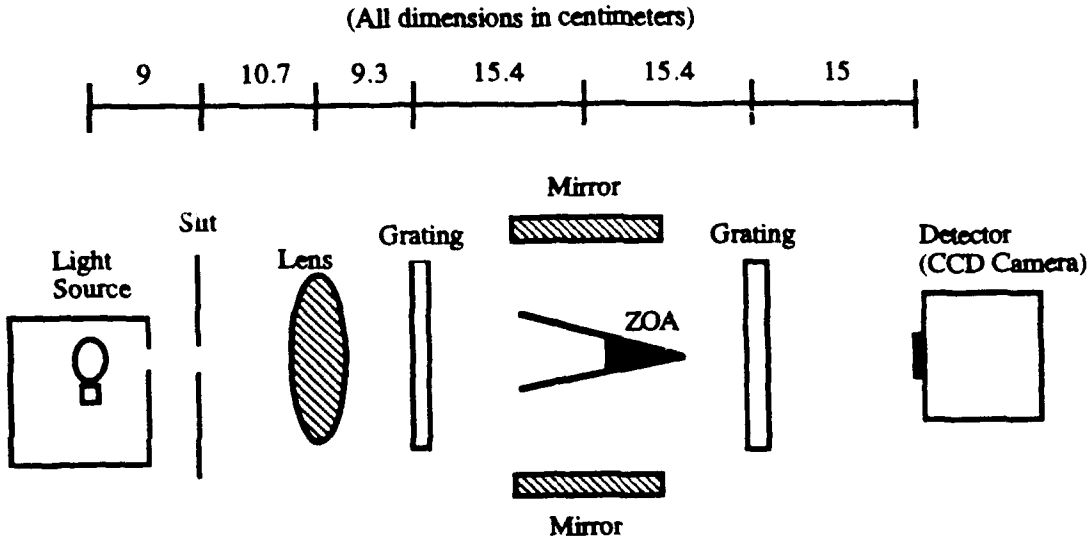

Figure 4.2. Sodium Source Experiment Dimensions.

be the result of interference from the two different arms of the interferometer. It is believed that interference between the two lines of the yellow doublet was observed.

This behavior is depicted in Figure 4.3. The figure shows only the paths for the positive first order diffractions through the first grating to show how the interference

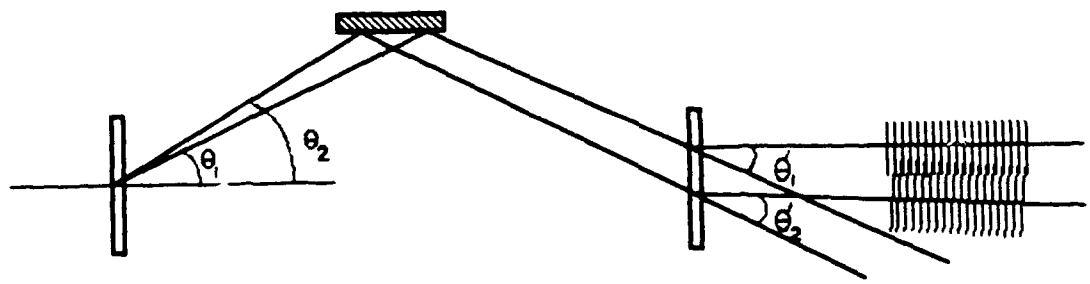

Figure 4.3. Sodium Doublet Interference.

pattern could appear when one mirror is covered. Two wave fronts propagate through the apparatus, each corresponding to one of the spectral lines of the sodium

doublet. The two fronts are diffracted at slightly different angles at both gratings. This also makes their path lengths slightly different, which places the wave fronts out of phase at the detector. However, it is the difference in the direction of propagation of the wave fronts which produces the interference pattern. Because the angle of diffraction for both wave fronts is almost equal, they intersect at very steep angles. This produces an interference pattern along only one path of the apparatus. To eliminate this problem, the sodium source was replaced with a mercury discharge lamp.

The mercury discharge lamp provided several bright lines to be considered for use. The green line appeared brightest to the eye, and therefore was considered first for use in the experiment. However, its close proximity to the bright yellow doublet meant that there might be more images than desired visible at the detector. The blue line, although more difficult to detect by the human eye, had sufficient intensity to be measured photographically. Additionally, because of its wavelength of 4358 Å, the blue line was diffracted at a sufficiently small angle so that only it and the much fainter violet line at 4047 Å would strike the mirrors if they were positioned to reflect its first order diffractions. Therefore, only the blue and violet lines would be reflected to the second grating and into the detector. A blue transmission filter eliminated the violet line and was placed in the apparatus behind the collimating lens. This placement eliminated other wavelength images in the visible region which did not strike the mirrors on diffraction through the first grating, but whose images could

reflect off other surfaces in the laboratory and produce false images on the detector. Figure 4.4 depicts the apparatus using the mercury arc lamp as source.

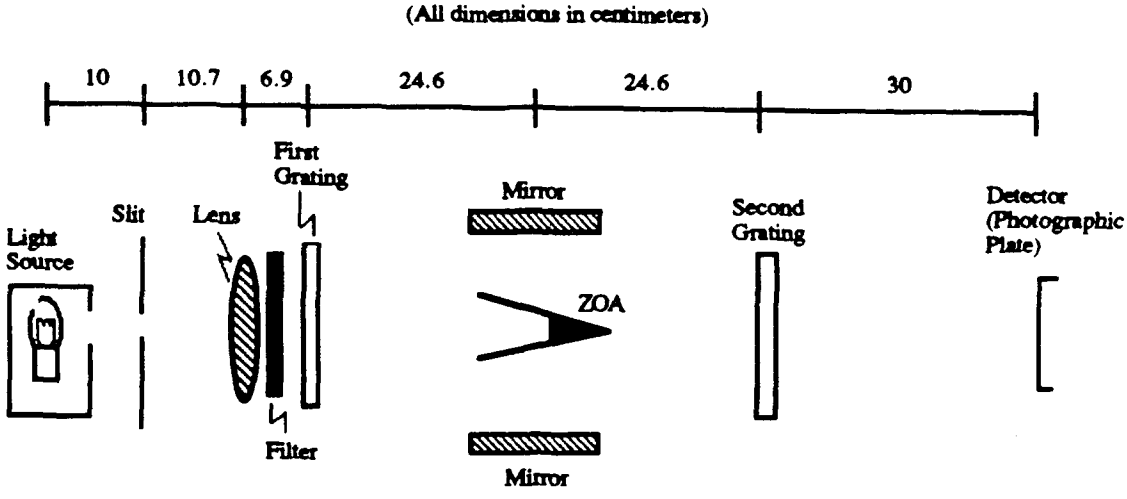

Figure 4.4. Mercury Source Experiment Dimensions.

As with the sodium lamp, no fringes were detected with the mercury source. To explain why, a more detailed look at the theory was in order. Figure 4.5 supports the following calculations concerning the overlap of two wave fronts of equal wavelength.

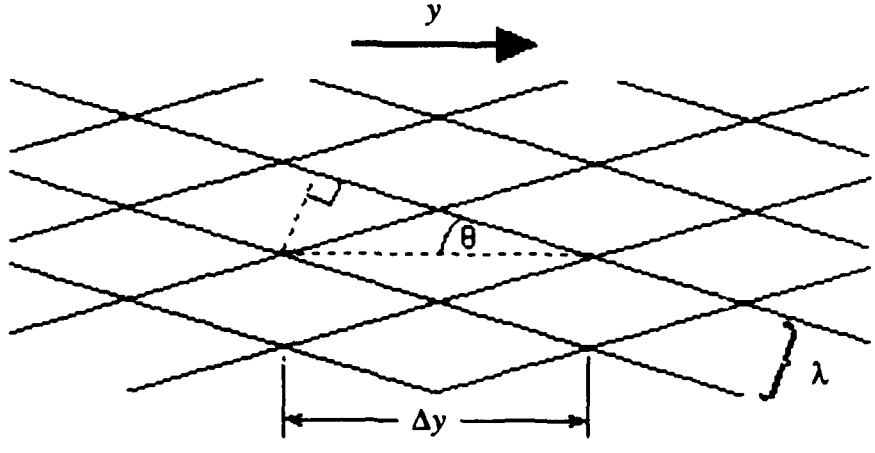

Figure 4.5. Separation of Fringes.

Assuming that the apparatus is perfectly aligned, the direction of propagation of the two wave fronts make the same angle but of opposite sign with the axis of the apparatus. Each wave front itself intersects the *y* axis with an angle θ. The angle between the two wave fronts is then 2θ. The sine of θ is the wavelength λ divided by the distance Δy between successive maxima. The distance between successive maxima for $\theta = 1°$ and $\lambda = 5000$ Å is about equal to 30 microns. If each wave front makes an angle of only 0.5° with the *y* axis the distance between maxima is still less than 60 microns. The gratings used were reported as having ruling densities of 25,100 and 25,000 lines per inch. A first order diffraction through both of them would produce an angle of 0.13° between the direction of propagation and the axis of the apparatus. This would make the angle between the two wave fronts twice that amount, or 0.26°. Such an angle would produce fringes that were approximately 220 microns (0.22 mm) apart. Although this is not an easily visible separation, it is one that should appear on the photograph. This again assumed that the alignment in the apparatus was perfect.

To resolve the issue of grating differences, several gratings, including those used in the experiment, were measured for ruling density with a spectrogram comparator. The two gratings used in the experiment were measured to have the same ruling density of 25,200 ± 70 lines per inch. This is not unexpected since both were replica gratings from the same master. In such gratings the rulings are transferred from a master to a blank through a collodion which is then fixed to the blank. The collodion has a tendency to shrink with age, increasing the ruling density. To the best

measurement capability possessed, the gratings were indeed equal. The difficulty in creating fringes must then have been due to a difference in the optical path length along both routes for the divided wave front.

If the alignment was not perfect, the wave fronts could still be leaving the second grating at near parallel directions of propagation. However, they would not be in phase due to a difference in optical path length. The coherence length of the mercury blue line at atmospheric pressure is on the order of 1 mm. Therefore, if the difference in path lengths approaches half that length, fringes will not occur. This is most likely the problem since mirror positioning is so critical to path length and difficult to verify accurately. If one mirror's distance from the axis of the apparatus differs by 0.5 mm from that of the other, the resulting optical path difference would be more than 1.0 mm. Since a mismatch in optical path length was suspected as the problem, a change to a source of greater coherence length was the next logical step.

A class II helium-neon laser with a wavelength of 5435 Å was next used as the source. The apparatus remained the same except for changes in position and removal of the slit and the blue filter. The laser was fitted with a beam expander, and the beam was passed through an aperture stop whose area was equal to that of the ruled portion of the first grating. The laser was placed approximately two meters from the first grating at the same height. It was aligned with the axis of the optical table by placing vertical pegs at far ends of the table, the first with a height barely touching the beam. The laser position was shifted until the beam struck both peg tips. The laser was leveled by assuring that its beam height remained constant. The grating was

again checked to be sure the rulings were vertical. The mirrors and second grating were aligned simultaneously. The second grating was placed in its approximate position, and the mirrors were slid along their axis on the table so that the diffracted beam struck their centers. The mirrors were then canted about the horizontal axis until the beams remained level. Next they were canted about the vertical axis until the reflected beams intersected the zero order transmission through the first grating on the face of the second grating. The second grating's rulings were verified to be vertical in the same manner as the first. For fine tuning, a target was placed approximately three meters beyond the second grating. If the grating and mirrors were properly positioned, the beam transmitted directly through both gratings and the two diffracted beams would overlap at any position beyond the second grating. By trial-and-error the beams were made to overlap as perfectly as was discernible with the human eye. Finally, the beam expander was inserted between the laser and the first grating and aligned so that its expanded beam was centered on the grating. The aperture was then inserted in front of the grating. The ZOA was reinstalled and the photographic plate was positioned about 40 cm behind the second grating to eliminate all but the desired wave fronts from striking the plate. The final setup is depicted in Figure 4.6. The first photograph showed an easily distinguishable fringe pattern. The next two photographs were taken covering each of the two mirrors individually to eliminate one of the wave fronts. As expected the fringes were not present. Finally, a fourth photograph was taken, again with both paths open. Fringes similar to the first photograph appeared. The capability to divide a single wave front

on two paths using a grating and recombine it to produce interference fringes was thus demonstrated. This capability was now applied to the design of an instrument suitable for use in the far ultraviolet.

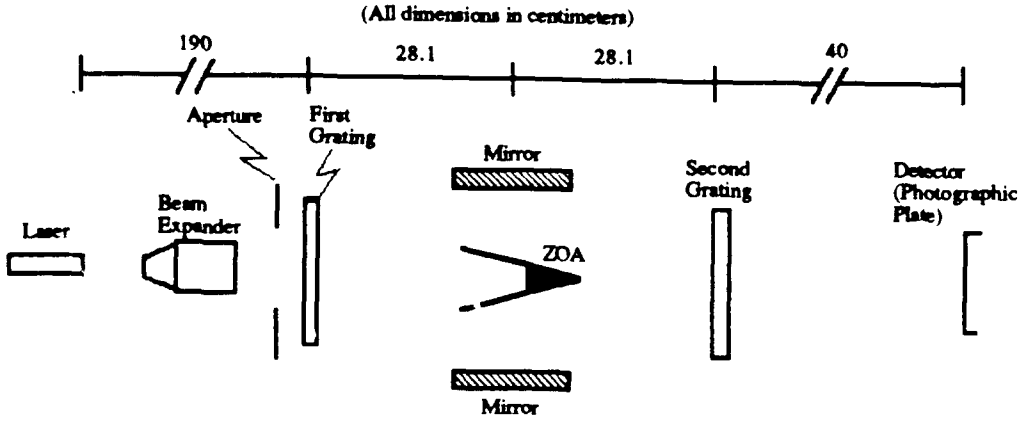

Figure 4.6. Helium Neon Laser Source Experiment Dimensions.

B. REFLECTION GRATING INTERFEROMETER

The reflection grating interferometer was designed to meet several specific requirements.

1. Operate in the far ultraviolet (reflective surfaces only)
2. Be sensitive to low intensity atomic emissions (minimize losses)
3. Have high resolution across a narrow bandwidth
4. Be compact and lightweight
5. Be suitable for a space flight environment

Additionally, because of the problems encountered in aligning an apparatus with two gratings and verifying exactly equal ruling densities, use of a single grating was preferred. Designs for grating interferometers, including some with all reflective optics for use in the far ultraviolet, have been explored by other investigators (Kruger et al., 1972; Fonck et al., 1978). However, these made use of several gratings and a minimum of four reflections. A major goal of the new design was to minimize losses. In the far ultraviolet this requires minimizing the number of reflections. First efforts at design were centered on the Rowland circle mount because of its familiar properties.

To maximize the fringe contrast with the available intensity of incoming radiation, it is necessary that the recombined wave fronts be of equal intensity. Therefore, the first design effort was on using the positive and negative first order diffracted beams, as in the transmission grating trials. Using a spherical concave reflection grating and placing the slit on the plane of the Rowland circle resulted in the output beams coinciding with the input slit. Figure 4.7 shows how light entering the slit is divided into positive and negative first order diffractions at the grating. It is then reflected off planar mirrors placed on the circumference of the Rowland circle and normal to the reflected wave fronts. The grating again diffracts the reflected wave fronts so that the positive first order of one and the negative first order of the other are recombined. The recombined wave front counterpropagates with respect to the incoming wave front. The design is the same as the two transmission grating prototype, but it is folded back onto itself. Since the slit and detector cannot be

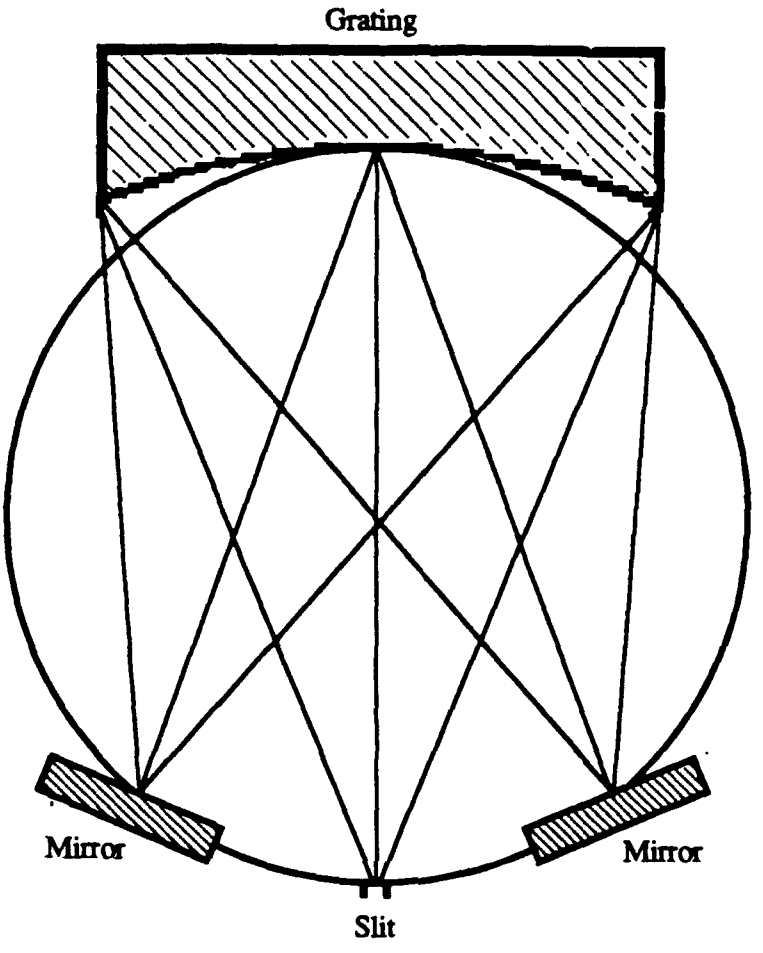

Figure 4.7. First Order Diffractions.

collocated, the design is impractical. The alternative used by Kruger et al. in their design with a plane grating was to move the slit vertically off-axis so that the slit was above the detector.

Moving the slit off the plane of the Rowland circle was next explored. When the slit is placed above the plane of the Rowland circle, the first order diffractions lie an equal distance below the plane. It is possible to recombine the divided wave front by properly positioning mirrors to reflect the image onto the surface of a second

grating. However, this adds the additional problem of trying to properly position the mirrors and second grating in relation to the first grating. The two grating design is shown in Figure 4.8.

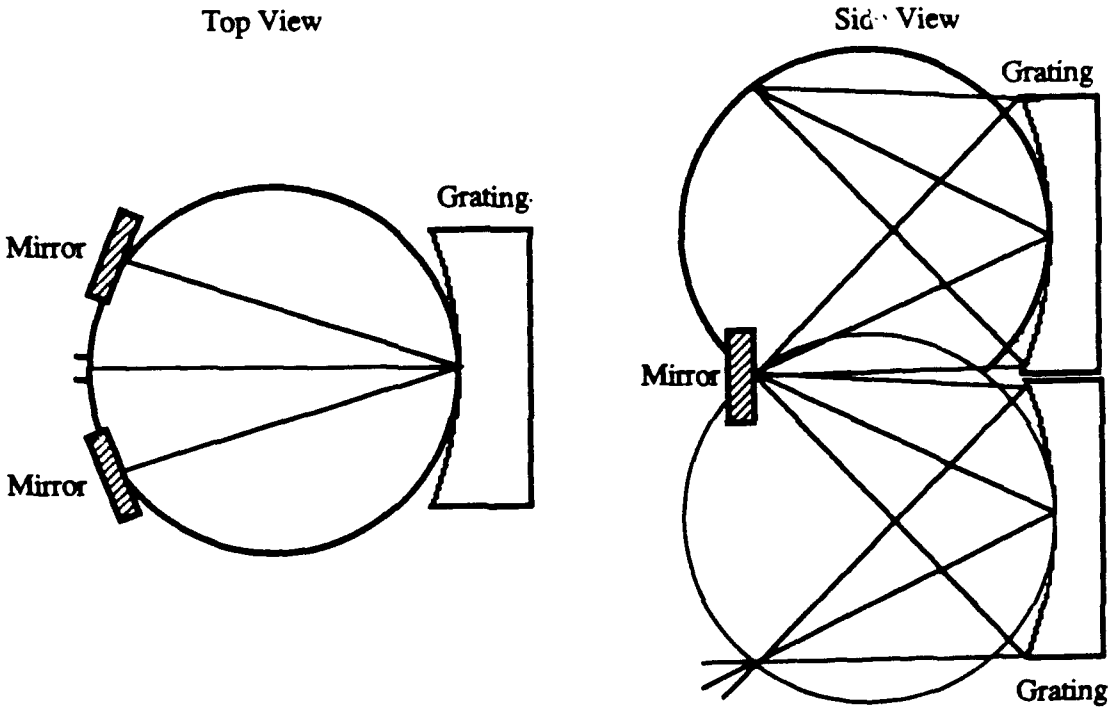

Figure 4.8. Two Grating Off Plane Design .

Another possibility was to leave the slit on the plane of the Rowland circle and to reflect the divided wave fronts above the plane and then back down to the grating by using an extra mirror on each path. This design is depicted in Figure 4.9. Although feasible, the design adds an additional reflection along each path and requires a difficult alignment of the mirrors in pairs in order to maintain equal optical path lengths and to eliminate distortion.

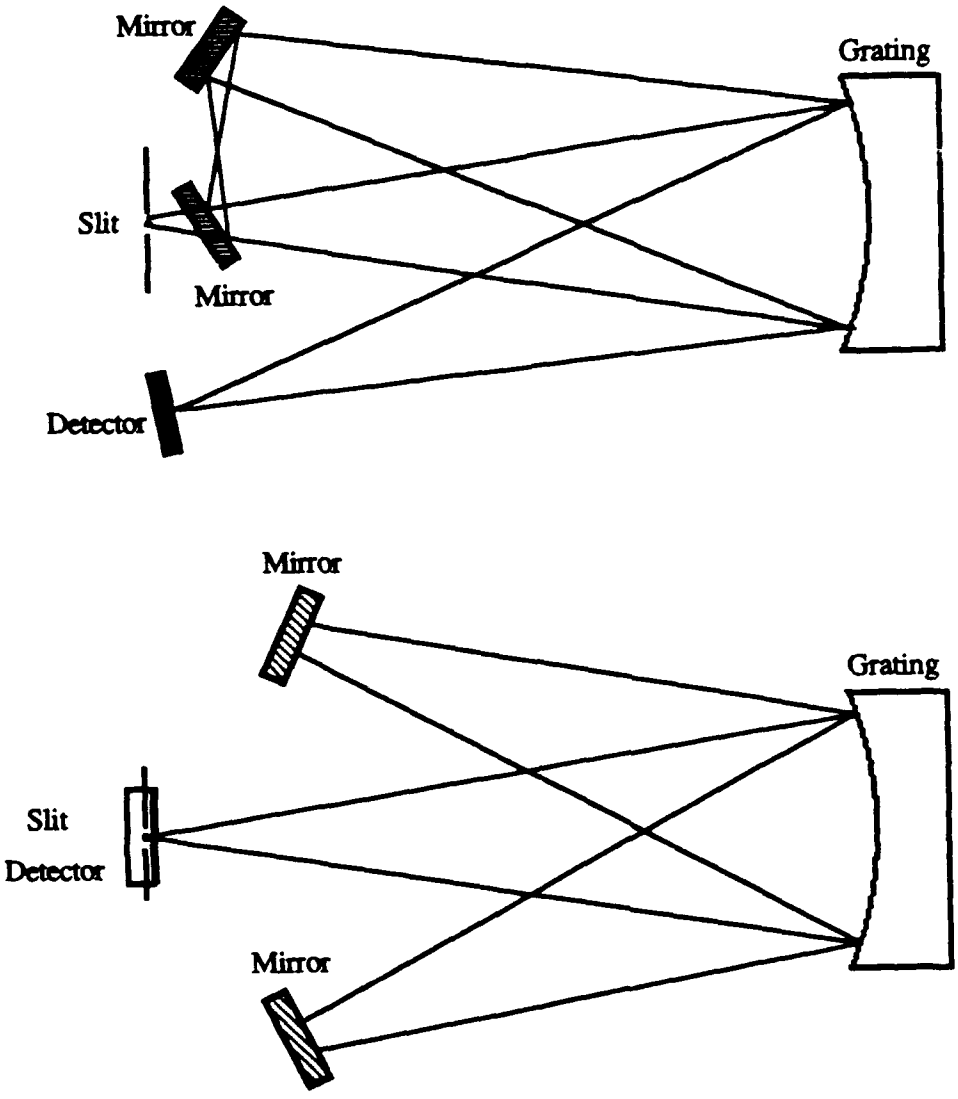

Figure 4.9. Mirrors for Off Plane Imaging.

Next, the possibility of operating entirely in the plane of the Rowland circle was explored. The design moves the slit off the normal to the grating and considers recombining different order diffractions of the incoming wave front. Figure 4.10 is a design in which the zero order and positive first order diffractions are recombined. Light leaving the slit travels along path *a1* to the grating. The zero order diffraction

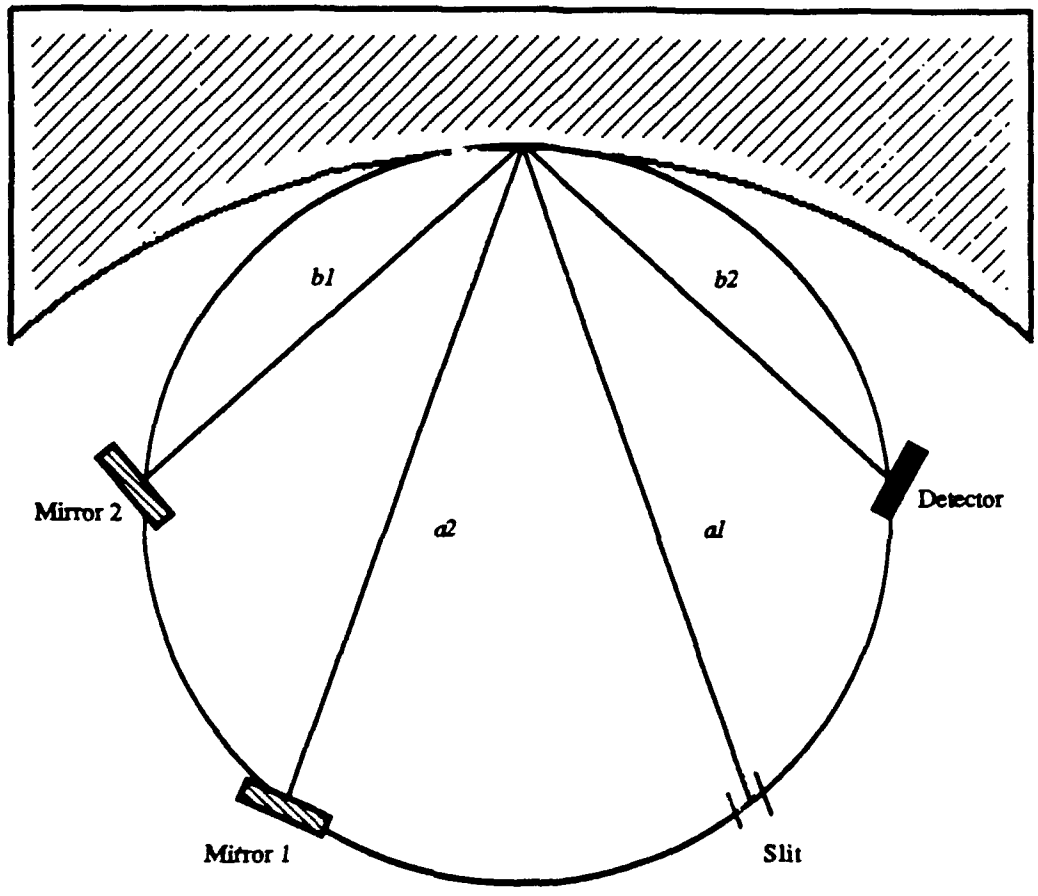

Figure 4.10. Rowland Circle Planar Mount.

travels along path *a2* to *mirror1* and is reflected back along the same path to the grating. Its positive first order diffraction then travels along path *b2* to the detector. The second wave front comes from the initial first order diffraction from the grating. It travels along path *b1* on leaving the grating, is reflected off *mirror2* back along the same path and finally exits along *b2* as the zero order diffraction from the grating.

This design has several important features. It uses two diffractions, the zero and positive first orders along each path. This means that the two paths will not only have equal intensities, but that a large portion of the available intensity is being retained.

It uses only one grating for all diffractions, so alignment and variability of ruling density problems are reduced. Selection of the incident angle controls the bandwidth of wavelengths sampled for a given ruling density of the grating. Since the entire design is on the Rowland circle and symmetric, a mechanical system for realignment of the apparatus to vary the incident angle would not be difficult to design or to build. There is, however, one significant drawback to this design. The path lengths of the two divided wave fronts are not equal. Paths *a1* and *a2* are equal as are paths *b1* and *b2*. The paths travelled by the two wave fronts after the first diffraction are then $2a+b$ and $a+2b$. Since the path lengths are not equal, identically paired wave groups from the single source would arrive at the detector at different times. Overlap would occur in uncorrelated wave groups and fringe contrast would be low or nonexistent.

In an attempt to compare the differences in path lengths, angles of first order diffractions were calculated for different angles of incidence. The results appear in Table 4.1. It was hoped that an incident angle could be selected so that the difference in path length would be less than the coherence length of the selected radiation. Positive first order diffractions were calculated first and yielded unsatisfactory results. Even with the slit placed only 5° off the grating normal, the positive first order diffraction angle was greater than 45°, so the path length difference was much larger than the coherence length of any source other than a laser. Negative first order diffractions were considered next. Calculations revealed that the angle of incidence could be selected so that the negative first order diffraction angle had a similar or

TABLE 4.1. DIFFRACTION ANGLES (IN DEGREES).

θ_i	θ_1	θ_{-1}
-5	47.67	-34.40
-10	55.67	-28.59
-15	65.64	-23.16
-20	83.83	-18.07
-25	none	-13.27
-30	none	-8.75
-35	none	-4.50
-40	none	-0.54
-45	none	3.15
-50	none	6.54
-60	none	12.34

even exactly equal value. The only constraint on placement then was the actual size of the optical devices to be used in the apparatus.

Figure 4.11 is a diagram of the setup using the negative first order diffracted beam. Light leaving the slit strikes the diffraction grating. The zero order beam reflects off *mirror1* and returns to the grating where the negative first order is diffracted to the detector. The second path uses the negative first order beam from the diffraction of the incident beam off the grating. It reflects off *mirror2* back to the grating where the zero order beam is diffracted to the detector. A quick attempt was made to identify the angle of incidence for which the optical devices could be

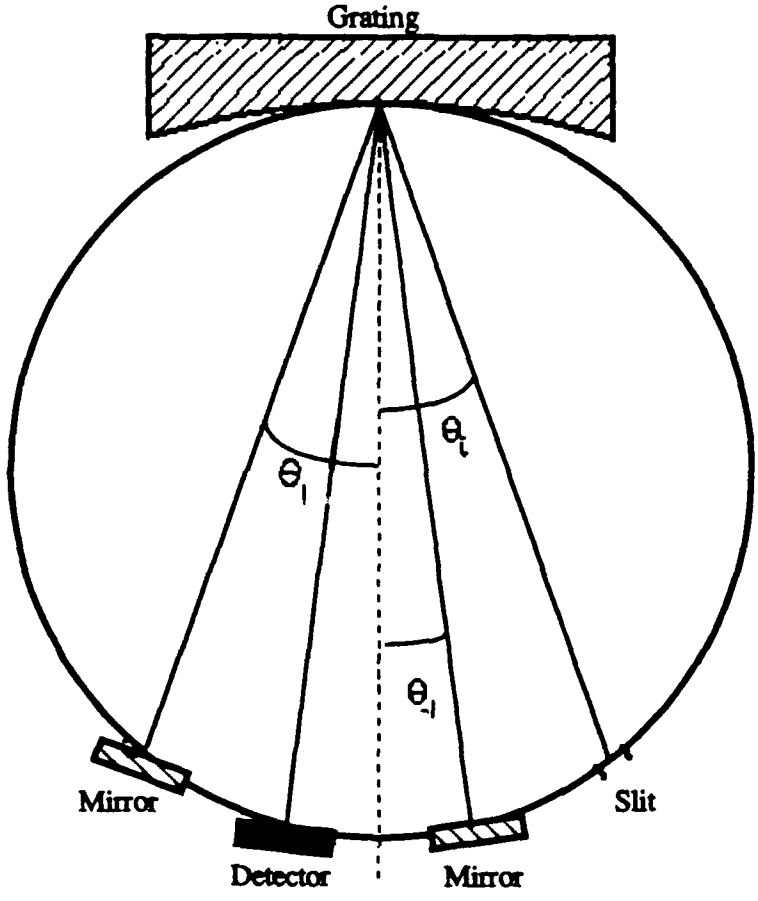

Figure 4.11. Calculation of Diffraction Angles.

positioned as closely as possible considering their size. Table 4.2 shows various results achieved for the calculations. Equation 3.1 was used to obtain the values. Positive angles are defined clockwise from the grating normal. The grating ruling density for calculations was 1200 lines per millimeter. The wavelength selected was 5435 Å, the wavelength of the helium-neon green laser. The results were examined to find the largest angular separation between the devices. The angle of incidence judged most efficient for separation of the devices was -29°. However, although the difference in path lengths was reduced, it was not eliminated. The radius of curvature of the

TABLE 4.2. ANGULAR SEPARATION OF DEVICES

θ_i	θ_{-1}	$\Delta\theta^*$	$\Delta\theta^{**}$
-24	-14.21	9.79	28.42
-25	-13.27	11.73	26.54
-26	-12.35	13.65	24.70
-27	-11.43	15.57	22.86
-28	-10.53	17.47	21.06
-29	-9.64	19.36	19.28
-30	-8.75	21.25	17.50
-31	-7.88	23.12	15.76

* slit to -1 mirror, detector to 0 mirror
** -1 mirror to detector

grating and hence the diameter of the Rowland circle was 20.14 cm. Chords off this diameter would therefore have lengths equal to the cosine of the angle made with the grating normal times that diameter. The difference in optical path lengths is twice the difference in the length of the chords. For the optimal setup with the angle of incidence at 29° this equates to a path difference of about 4.5 cm. The physical size of the optical devices made any improvement on the design impossible. The design process was at a standstill until the possibility of moving off the Rowland plane was again considered.

In calculating negative first order diffractions as a function of the angle of incidence, it was observed that the diffraction returned on the path of the incident wave front for one specific angle. If the slit were placed below the Rowland plane

with this specific angle of incidence, then the negative first order beam would be diffracted back on the same horizontal angle as the incident beam entered, but directly above it. This solved the problem of the separation of the optical devices. The slit and the second mirror could be placed at the same horizontal angle to the grating normal, but be separated vertically. The first mirror and the detector would be placed at the same horizontal angle on the other side of the normal and be separated vertically in the same manner.

This design, depicted in Figures 4.12a-c is symmetric about the grating normal, and the two path lengths of the interferometer are equal. Leaving the slit, the first

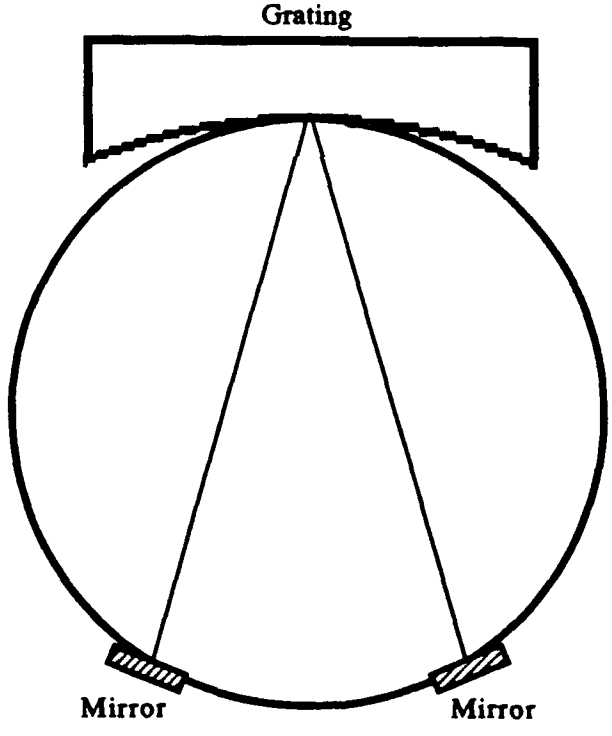

Figure 4.12a. Interferometer, Top View of Upper Beam Plane.

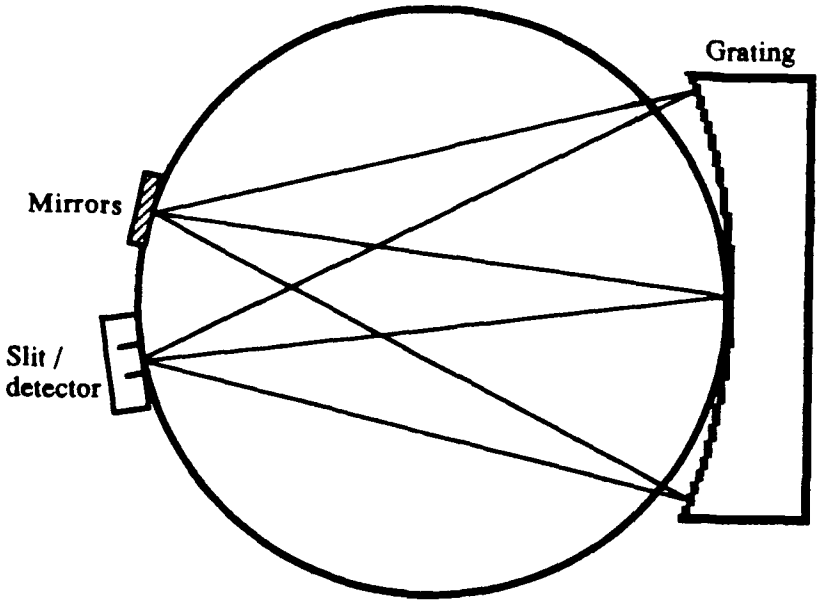

Figure 4.12b. Interferometer, Side View.

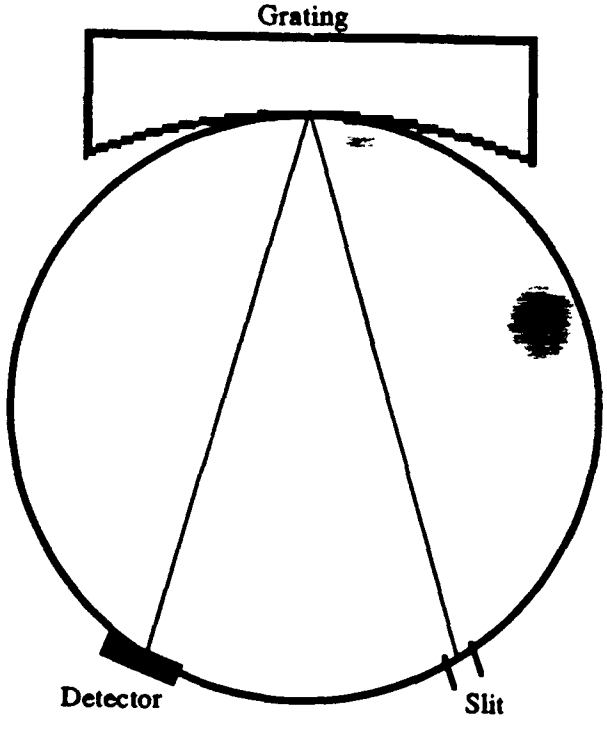

Figure 4.12c. Interferometer, Top View of Lower Beam Plane.

path follows the zero order beam as it is diffracted up and to the opposite side of the normal to the zero order mirror. It is reflected back to the grating where it is diffracted again. The path follows the negative first order diffracted beam as it exits to the detector. The second path follows the incident beam from the slit to the grating. On this path the negative first order diffraction is taken when the beam first encounters the grating. From the grating it travels to the negative first order mirror and is reflected back onto the grating. Here, in the second diffraction on this path, the zero order beam is diffracted to the detector.

The design reduces the number of reflections along each path to three. Additionally, it uses the zero and negative first order diffractions, thereby maintaining a large portion of the available intensity. For the design proposed, the incident and the negative first order beams were to come off the grating at the same horizontal angle, thus

$$\theta_i = \theta_{-1}$$

Substituting this condition into the general grating equation,

$$\theta_i = \sin^{-1}\left(-\frac{\lambda}{a} - \sin\theta_i\right)$$

and solving for θ_i yields

$$\theta_i = \sin^{-1}\left(\frac{-\lambda}{2a}\right) \qquad (4.1)$$

This gives the relation between the grating density, the observed wavelength, and the slit location. The general grating may be used as an approximation for the exact solution (Equation 3.2) if the assumption is made that the separation of the source

above the plane of the Rowland circle is small. The design can be made even more efficient by insuring that the zero and negative first order diffractions are the only ones produced by the grating. This is done by matching the grating ruling density to the wavelength selected for observation. If the angle of diffraction for the positive first order is greater than or equal to 90°, then the first order diffraction does not exist. Substituting this into the grating equation and solving for the incident angle gives

$$\sin\theta_i = \frac{\lambda}{a} - 1 \qquad (4.2)$$

Similarly, Equation 4.1 can be expressed as

$$\sin\theta_i = \frac{-\lambda}{2a} \qquad (4.3)$$

Equating the right hand sides of Equations 4.2 and 4.3 gives an expression for the minimum grating ruling density which eliminates the unused diffraction orders, thus

$$\rho = \frac{1}{a} = \frac{2}{3\lambda} \quad .$$

This expression is then used to find the incident angle associated with the minimum grating density.

$$\theta_i = \sin^{-1}\left(\frac{1}{3}\right) \quad .$$

Therefore, the horizontal angle that separates the slit from the normal to the grating will always be 19.47°. To examine the line profile of the 1304 Å oxygen line for example, the minimum ruling density should be 5112 lines per millimeter. For the

experiment with the helium-neon green laser source, the minimum ideal ruling density would be 1228 lines per millimeter.

For the actual experiment conducted, intensity at the source was not a concern. Therefore a more commonly manufactured grating with a ruling density of 1200 lines per millimeter was used. This was a holographic grating with a sinusoidal groove profile. The dimensions of the grating are described in Figure 4.13. The grating was mounted so that it had micrometer translation capability on all three axes and rotation capability around both axes perpendicular to the grating normal. The grating was secured in a machined plate with set screws on two axes. The plate had a small handle on the back and was locked into the mount with a threaded ring which held it firmly against the face of the mount. If the ring was loosened, the plate could be rotated by hand about the third axis, the grating normal. (Figure 4.14)

The zero and minus one order mirrors were one inch diameter plane mirrors, flat to 0.1 wavelength. They were secured with three brass hold-downs onto a mount with a second plate directly behind the mounting plate on a long rod, all machined from a single piece of solid, cylindrical stock. Three set screws 120° apart in the mounting plate could be turned against the backing plate to apply slight pressure changes to the face of the mount. The shaft of this mount fit into a stock bracket which allowed small translations on three axes and rotation around two. (Figures 4.15 & 4.16)

Since mirror position actually represented the lengths of the two paths for the interferometer, it was apparent that stabilizing their mounts was required to get stationary fringe images. A special bracket of aluminum pipe, channel and angle stock was constructed for this reason. Columns made from the piping supported the channel and were half filled with lead shot to provide damping and to add mass to

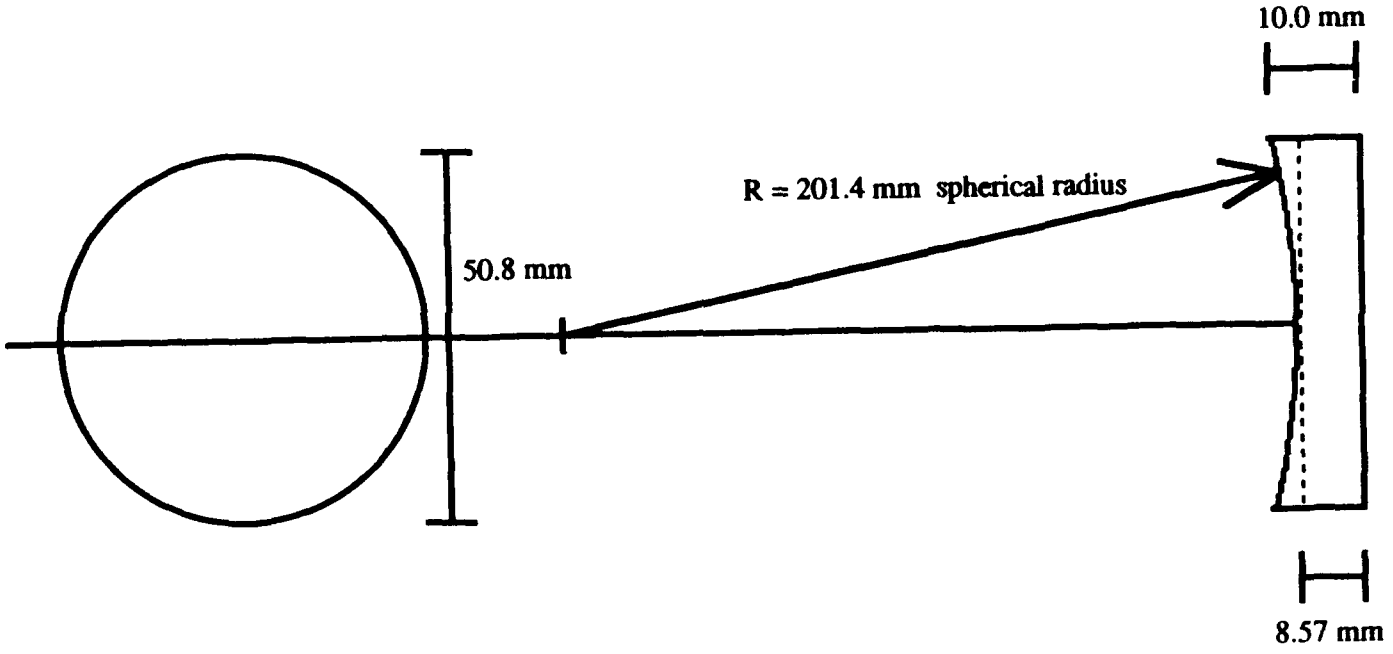

Figure 4.13. Grating Dimensions.

Figure 4.14. Grating Mount.

the base of the structure. The bracket can be seen in Figure 4.17, a photograph of the experimental setup. The channel was slotted where the angle stock was attached to permit macroscopic adjustment of both translation and rotation on one axis. The angle stock sections were slotted to permit translation on a second axis. The base of the mirror bracket was slotted where it connected to the angle stock to provide a

Figure 4.15. Mirror Mount.

Figure 4.16. Mirror in Bracket.

second rotational axis and the third translation axis. In this way macroscopic adjustments could be made to the apparatus along one axis at a time. Both the angle sections and the actual mirror brackets had machined feet which permitted them to be locked down tightly. The circumference of the pipe served this purpose for the

Figure 4.17. Experiment Setup.

channel. The channel itself was held down with a threaded rod which extended through the pipe to the optical table also locking down the piping. The entire structure proved to have an additional advantage in that it held both mirrors to the same base of support.

The helium-neon laser was used as the source. A Sharp 20X standard microscope objective lens with a numerical aperture of 0.40 was fixed to the end of the laser as a beam expander for the actual experiment, but was not used during alignment. The laser was attached to a small table which allowed leveling through three set screws. Translation was done by hand.

For initial alignment no detector was used. Instead a white target board was placed behind the expected detector location to observe the exiting recombined wave fronts as they diverged beyond the focal point on the Rowland circle. Later, a CCD camera without lens (Figure 4.18) was used as the detector. Images were portrayed on a black-and-white monitor and photographed directly from the screen.

Figures 4.17 and 4.19 are photographs of the entire setup. The first is a view from behind and to the side of the grating. Figure 4.19 displays the apparatus looking into the grating down the axis of its normal. It shows the symmetry of the design. The two mirrors and the source all occupy the same location in different quadrants of a two dimensional coordinate system. The plane of the system is perpendicular to the grating normal with the origin for the horizontal and vertical axes defined at the intersection of the plane and the normal. Figure 4.20 is a closeup of the mounted mirrors as seen looking directly over the top of the grating bracket.

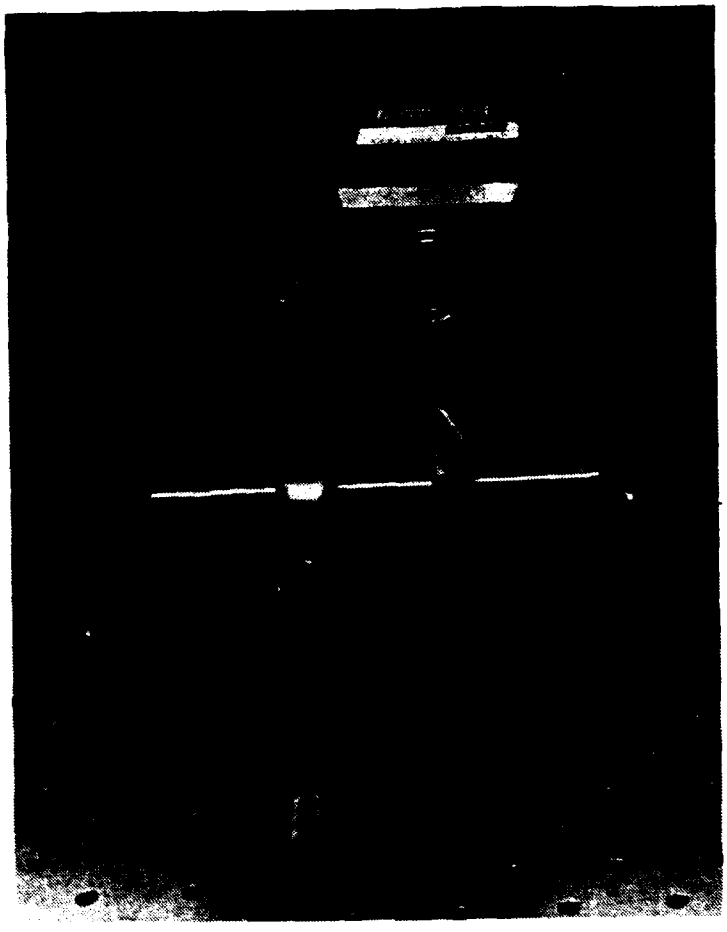

Figure 4.18. CCD Camera.

Alignment was begun by placing the laser near the axis of the grating normal and at the maximum distance from the grating that the optical table would allow. The aperture of the laser was adjusted to the same height as the grating center. The laser beam was again leveled by insuring the beam maintained a fixed height along the optical table. The grating was now rotated about its vertical and horizontal axes to return the laser beam back to the source. The grating was also rotated about its normal to align the rulings parallel with the vertical axis. This was done by assuring

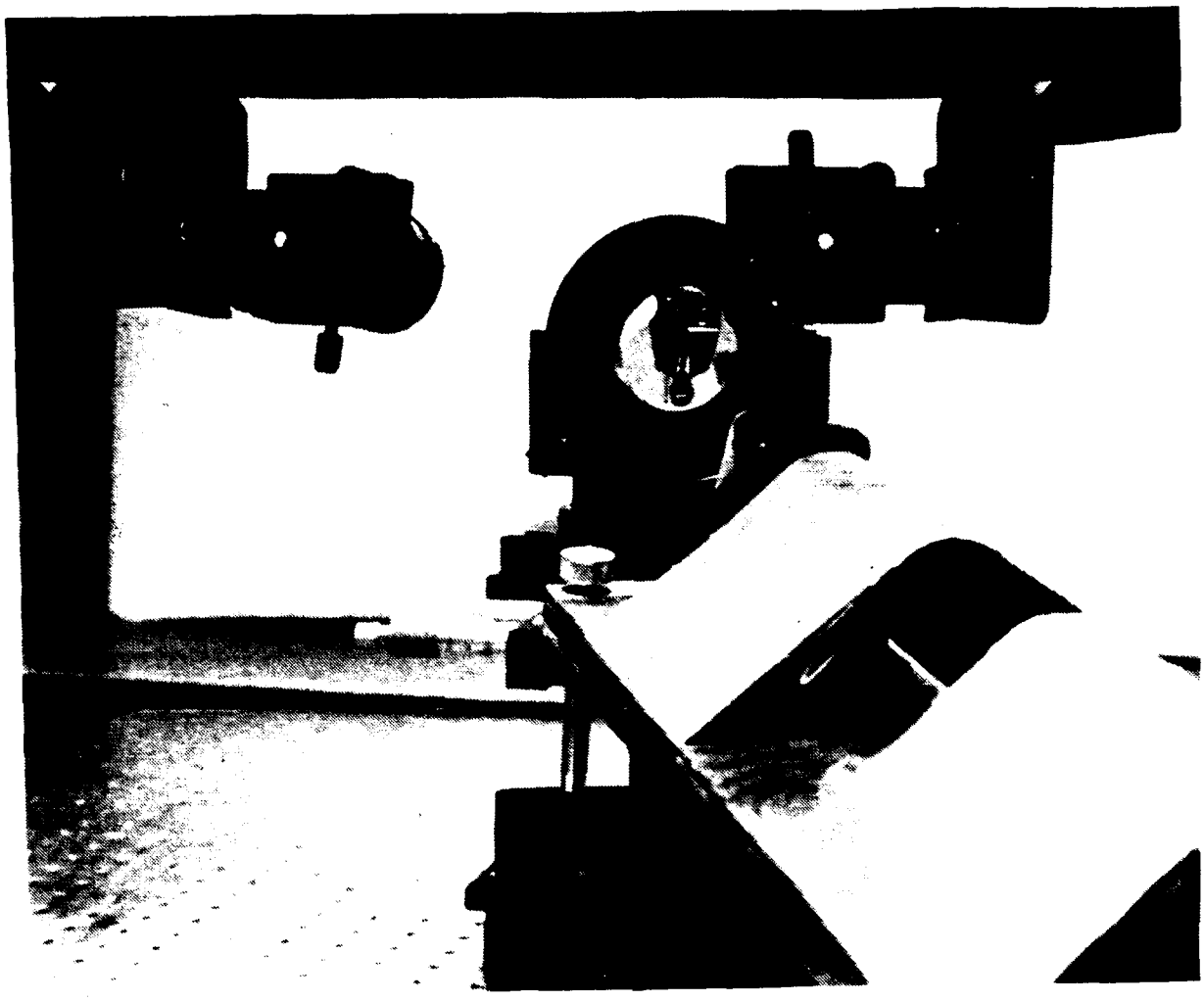

Figure 4.19. Experiment, Grating Axis View.

that both first order diffractions were at the same height as the laser beam. This fixed the location and orientation of the grating.

Next the beam expander was fixed to the laser, and the laser was positioned as the source. The laser aperture was approximately three centimeters below the plane of the Rowland circle. The horizontal angle from the normal to the source did not need to be measured. The source was adjusted so that its beam was centered on the grating and its first order diffraction focused directly above it. This was accomplished by scribing a vertical line on a clear piece of plastic fixed to a height gauge. If the

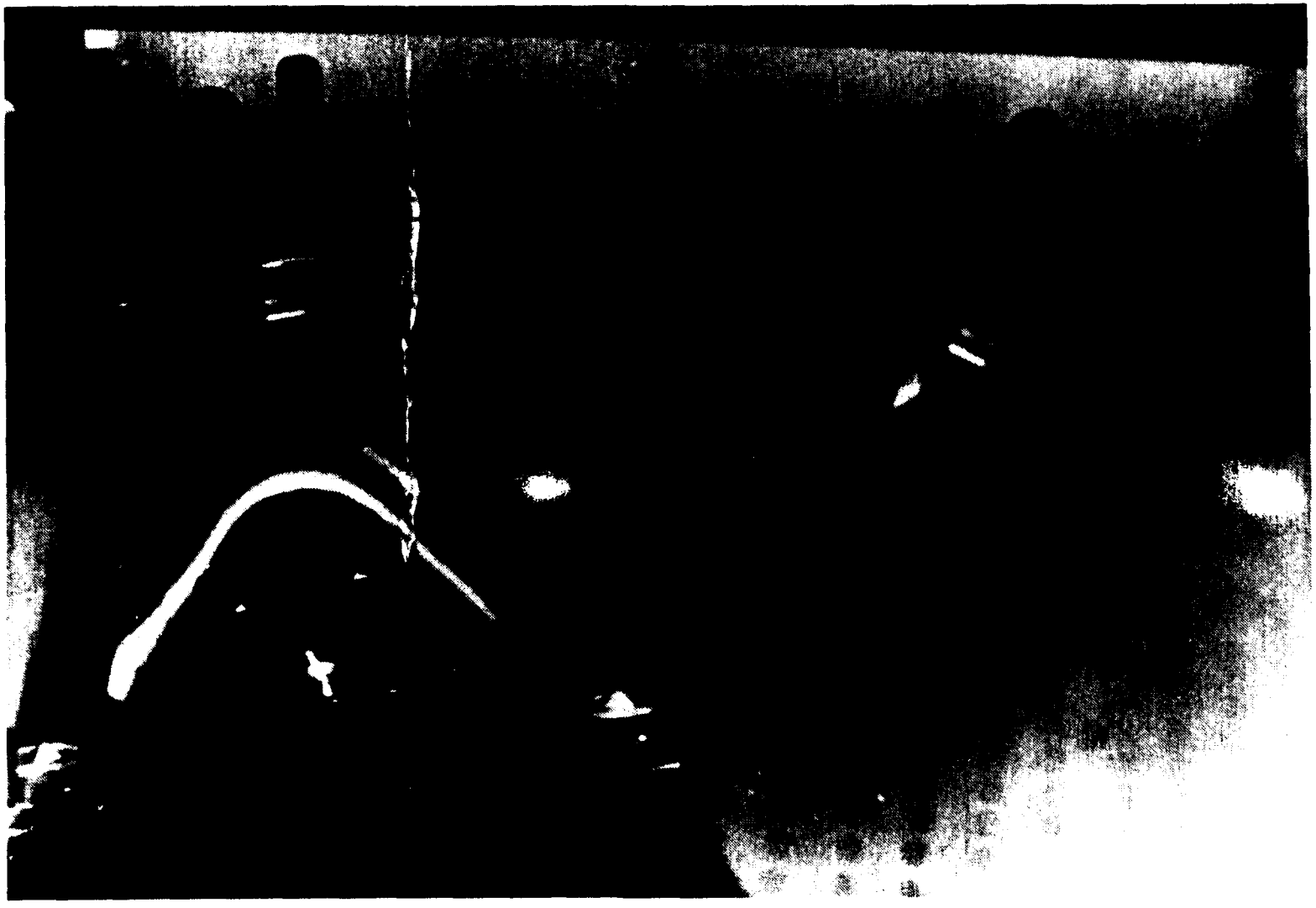

Figure 4.20. Mounted Mirror Positions.

incident and diffracted rays defined a vertical plane, then the source was properly positioned.

Alignment of the mirrors was also accomplished visually. The zero order mirror was done first. On striking the grating a second time, the zero order beam should return to the source. The mirror was adjusted to make this the case. Finally, the negative first order mirror was adjusted so that its image on leaving the instrument directly overlay that of the zero order mirror. This brought the two divided wave fronts back onto parallel paths.

The distance from the source and both mirrors to the grating was calculated using Equation 3.2 and solving numerically for the incident angle of 19.34°. The cosine of this angle times the diameter of the Rowland circle gives the chord length from the grating to the devices, 19.00 cm. It was also considered that the vertical angle above the plane might have an effect on the distance. The chord of the horizontal angle lies in a vertical plane which cuts a circular cross section of the sphere whose surface is tangent to the grating. The chord formed by the vertical angle was calculated to be 18.69 cm. Both values were tried in the experiment.

V. RESULTS

With the helium-neon laser as the source, fringes were obtained quite easily. The image from each of the different paths was not a point at the exit location of the apparatus. Instead, because of the astigmatism associated with the spherical grating, each appeared as an approximately vertical line. The two overlapped images formed an upright X at the tangential focus. The circle of least confusion was between that and a horizontal X in the sagittal plane. The detector was not placed at any of these three locations, but much farther away from the grating. Since the spherical mirror focused the expanded beam back into a small image and the fringe pattern lay only in the crossed portion of the X, the fringe pattern was not recognized at first. The pattern was first observed on a screen placed about one meter from the grating, where the image had greatly expanded.

The fringe images first observed were hyperbolic in nature, indicating that the two paths of the interferometer were not sufficiently equal. The initial position of the mirrors and source was 19.0 cm from the grating. Adjustment of the two mirrors' positions along their normal axes yielded elliptical fringes, but this resulted in an obvious difference in the optical path lengths. When the source and mirrors were placed 18.7 cm from the grating, elliptical fringes were obtained immediately. The CCD camera was initially placed about 75 cm from the grating. Any disturbance of a single mirror caused the fringe pattern to disappear until the disturbance damped

out. Tapping the source or the optical table caused the fringes to vibrate but not to disappear. These two results seem trivial but have important consequence for application design of the interferometer. Disturbances that affect only one path of the divided wave front are fatal to fringe formation. Those that impact both paths equally may disturb the fringes, but their image is not totally lost. For application, this means that the mirrors and detectors should not be anchored individually, but as a group. Then any external disturbance to the system would not impact severely on the interferometer's operation.

Figures 5.1 and 5.2 are photographs of the television monitor picture showing the fringes. It is important to note that the ellipse of the fringe pattern is tilted and not vertical. These photographs were taken with the camera mounted on its side, so that the horizontal and vertical axes are exchanged. The long axis of the ellipse lies along the length of one of the overlapping images. To determine why, the overlapping images themselves were examined more closely. Behind the sagittal plane both images are nearly horizontal lines. The individual sharpness or focus of those lines varies differently as distance from the grating increases. Moving back from the sagittal plane, the image from the mirror above the source is sharper. As the images are traced back, they reach a point where both appear equally out of focus. Then the image from the mirror above the exit becomes sharper. In either case, the ellipse of the fringe pattern lies with its major axis along the less focused image. If the detector is placed where the images are equally focused the ellipse of the fringe pattern is horizontal.

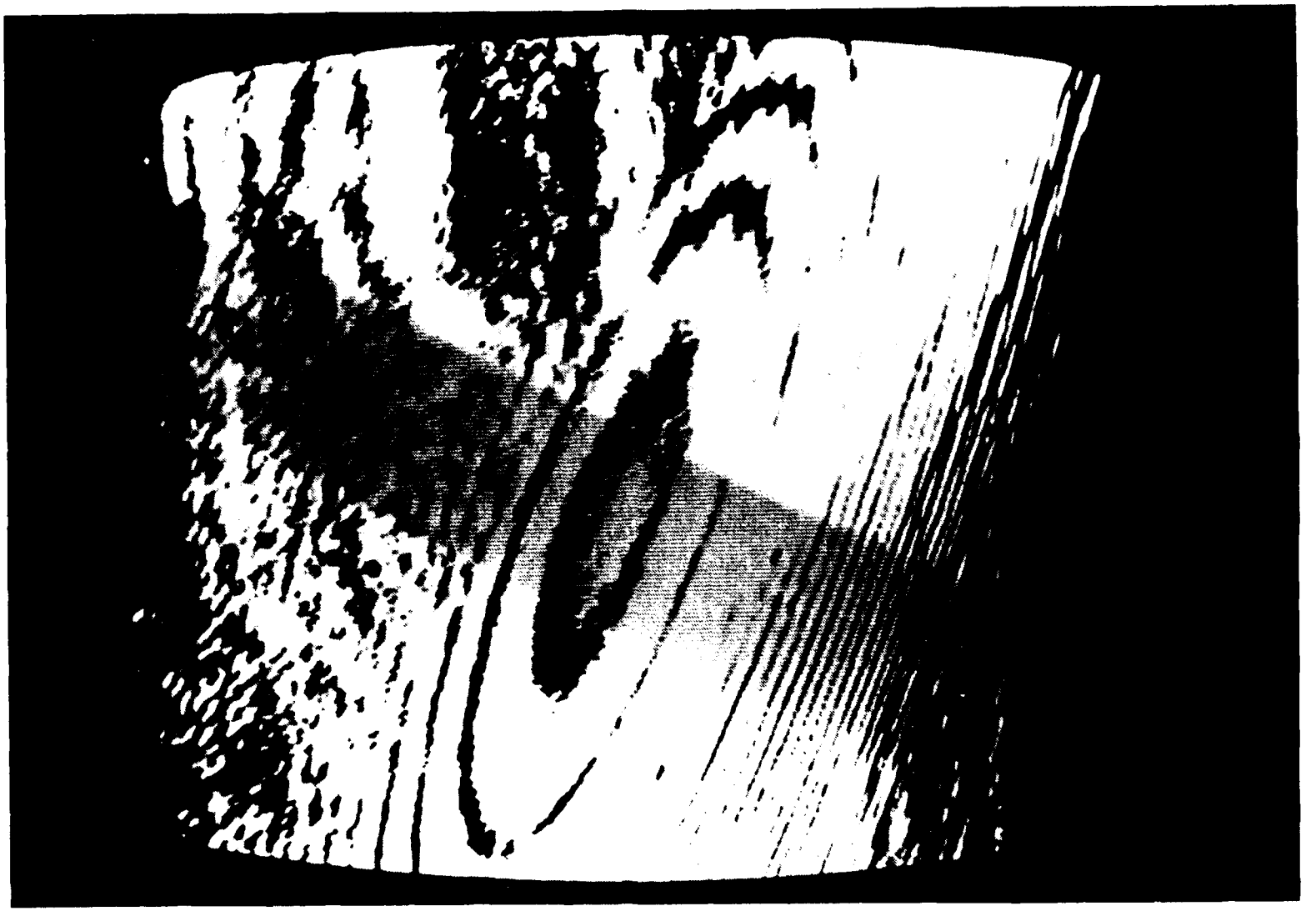

Figure 5.1. Fringe Pattern.

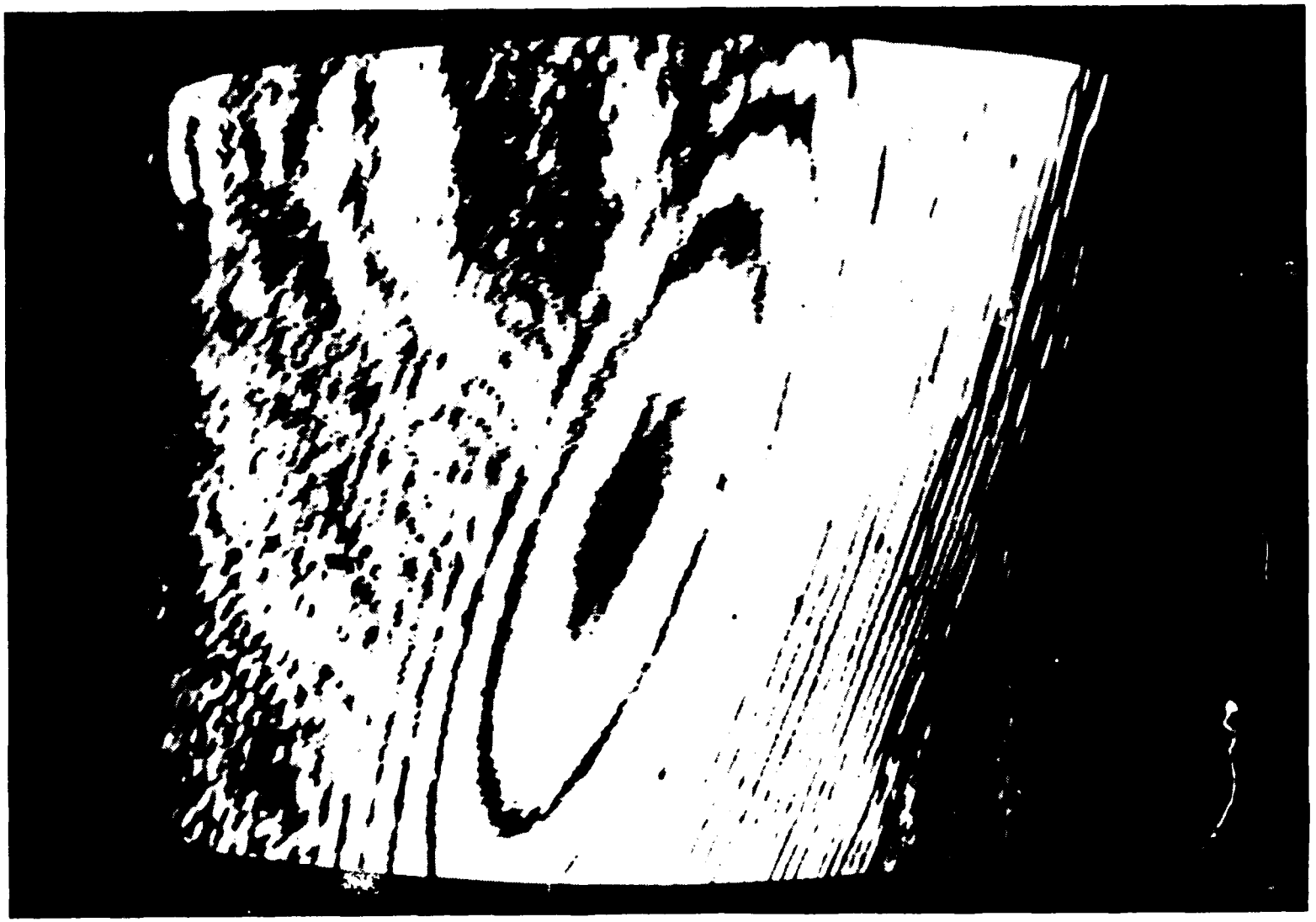

Figure 5.2. Fringe Patterns.

Adjustment of the interferometer paths can increase or decrease the fringe separation. Ideally, if the two paths were perfectly equal, the center maximum would become infinitely large and the pattern would disappear. Point sources would normally be expected to yield circular fringes. However, the pattern is always elliptical and not circular. This is because of the astigmatism associated with a spherical grating.

The fringe patterns that were obtained had sharp contrast between maxima and minima and were sufficiently stable for detection and measurement. The experimen using a helium neon laser source succeeded in producing an interference fringe pattern suitable for spectroscopic analysis.

VI. CONCLUSION

A. SUMMARY OF FINDINGS

A new far ultraviolet interferometer was designed, built, and tested using a helium neon laser as the source. The interferometer uses a single spherical concave reflection grating to divide and to recombine incident wave fronts to produce interference. The interferometer selects wavelengths over a narrow band with high resolution. In the laboratory a high contrast elliptical fringe pattern suitable for spectroscopic analysis was produced.

The desired design features for the interferometer were met. Only reflective surfaces were used, so the interferometer can sample far ultraviolet emissions. The design maximizes use of available intensity by using only zero and negative first order diffractions and eliminating all other diffraction orders through appropriate selection of grating ruling density. Additionally, the design reduced the number of reflections along each optical path to three. Through positioning of the optical devices within the interferometer, only a narrow bandwidth of radiation is sampled. The development of fringe patterns for Fourier analysis can yield high resolution spectra. The interferometer is simple, lightweight, and compact. The fringe pattern was found to be sufficiently stable for sampling if the optical devices were on a single mounting structure making the instrument suitable for a space flight environment.

The fringe pattern was elliptical because of astigmatism associated with placing the slit, detector, and mirrors of the interferometer off-plane in a Rowland circle mount. Astigmatism in the design can be reduced by positioning optical devices closer to the axis of the grating in the interferometer if the grating ruling density is decreased. However, this has the undesirable effect of reintroducing the positive first order diffractions.

B. RECOMMENDATIONS FOR FURTHER RESEARCH

The current interferometer design was tested using a coherent source in the visible region. To verify the feasibility of using the design for spectroscopic analysis of far ultraviolet atomic emissions, several further experiments need to be performed. First, the optimal distance of the slit, detector, and mirrors from the grating should be determined through ray tracing and verified by obtaining a usable fringe pattern with an incoherent source. The problem in determining the correct distance lies with the astigmatism of the off-plane mount.

Development of a stable adjustable mounting system that connects the slit, detector, and mirrors so that all four devices move properly in relation to one another would make the interferometer "tuneable" for sampling different wavelengths. The basics for this design are already contained in Rowland circle mounts. This type of a mount need only be expanded to four devices rather than two.

A suitable detector for sensing far ultraviolet radiation and converting it to an usable data form needs to be developed. Once a suitable detector is produced,

verification of the capabilities of the interferometer in the far ultraviolet region can be accomplished.

LIST OF REFERENCES

Anderson, C.K., *Calibration of the Naval Postgraduate School Middle Ultraviolet Spectrograph and an Analysis of the OII 2470 Å and OI 2972 Å Emissions Obtained from Mid-Latitude Rocket Observations,* Master's Thesis, Naval Postgraduate School: Monterey, CA, September 1990.

Clayton, M.J., *Analysis of the Ultraviolet Emissions of Nitric Oxide from Mid-Latitude Rocket Observations,* Master's Thesis, Naval Postgraduate School: Monterey, CA, June 1990.

Fonck, R.J., D.A. Huppler, F.L. Roesler, D.H. Tracy, and M. Daehler, "All Reflection Michelson Interferometer: Analysis and Test For Far IR Spectroscopy," *Applied Optics,* vol. 17, p. 1739, June 1978.

Harlander, J., F.L. Roesler, and S. Chakrabarti, "Spatial Heterodyne Spectroscopy: A Novel Interferometric Technique for the FUV," Publication Number 15, Earth and Planetary Atmospheres Group, Space Science Laboratory, University of California, Berkeley, 1990.

Hecht, E., *Optics,* 2nd ed., Addison-Wesley: Reading, MA, 1987.

Jenkins, F.A., and H.E. White, *Fundamentals of Optics,* 4th ed., McGraw Hill: New York, 1976.

Krueger, R.A., L.W. Anderson, and F.L. Roesler, "All Reflection Interferometer for Use as a Fourier Transform Spectrometer," *Journal of the Optical Society of America,* vol. 62, p. 938, August 1972.

McCoy, R.P. and D.E. Anderson Jr., "Ultraviolet Remote Sensing of the F2 Ionosphere," *Effects of the Ionosphere on C^3I Systems,* National Technical Information Service, Springfield, VA, 1984.

Namioka, T., "Theory of the Concave Grating. I" *Journal of the Optical Society of America,* vol. 49, p. 446, May 1959.

Roesler, F.L., "Fabry-Perot Instruments for Astronomy," *Methods of Experimental Physics, vol. 12, Part A: Optical and Infared,* Academic Press: New York, 1974.

Samson, James A.R., *Techniques of Ultraviolet Spectroscopy,* John Wiley & Sons: New York, 1967.

BIBLIOGRAPHY

Anderson, C.K., *Calibration of the Naval Postgraduate School Middle Ultraviolet Spectrograph and an Analysis of the OII 2470 Å and OI 2972 Å Emissions Obtained from Mid-Latitude Rocket Observations,* Master's Thesis, Naval Postgraduate School: Monterey, CA, September 1990.

Banks, P.M., and G. Kockarts, *Aeronomy,* Academic Press: New York, 1973.

Chamberlain, J.W. and D.M. Hunten, *Theory of the Planetary Atmospheres. An Introduction to Their Physics and Chemistry,* 2nd ed., Academic Press: Orlando, 1987.

Chang, B.J., R. Alferness, and E.N. Leith, "Space-Invariant Achromatic Grating Interferometers: Theory," *Applied Optics,* vol. 14, p. 1592, July 1975.

Clayton, M.J., *Analysis of the Ultraviolet Emissions of Nitric Oxide from Mid-Latitude Rocket Observations,* Master's Thesis, Naval Postgraduate School: Monterey, CA, June 1990.

Fonck, R.J., D.A. Huppler, F.L. Roesler, D.H. Tracy, and M. Daehler, "All Reflection Michelson Interferometer: Analysis and Test For Far IR Spectroscopy," *Applied Optics,* vol. 17, p. 1739, June 1978.

Guenther, R., *Modern Optics,*, John Wiley & Sons: New York, 1990.

Harlander, J., F.L. Roesler, and S. Chakrabarti, "Spatial Heterodyne Spectroscopy: A Noval Interferometric Technique for the FUV," Publication Number 15, Earth and Planetary Atmospheres Group, Space Science Laboratory, University of California, Berkeley, 1990.

Hecht, E., *Optics,* 2nd ed., Addison-Wesley, Reading, MA, 1987.

Hines, C.O., I. Paghis, T.R. Hartz, and J.A. Fejer, eds., *Physics of the Earth's Upper Atmosphere,* Prentice Hall: Englewood Cliffs, NJ, 1965.

Jenkins, F.A., and H.E. White, *Fundamentals of Optics,* 4th ed., McGraw Hill: New York, 1976.

Kelley, M.C., *The Earth's Ionosphere, Plasma Physics and Electrodynamics,* Academic Press: San Diego, 1989.

Krueger, R.A., L.W. Anderson, and F.L. Roesler, "All Reflection Interferometer for Use as a Fourier Transform Spectrometer," *Journal of the Optical Society of America,* vol. 62, p. 938, August 1972.

Krueger, R.A., L.W. Anderson, and F.L. Roesler, "New Fourier Transform All-Reflection Interferometer," *Applied Optics,* vol. 12, p. 533, March 1973.

McCoy, Robert P. and D.E. Anderson Jr., "Ultraviolet Remote Sensing of the F2 Ionosphere," *Effects of the Ionosphere on C^3I Systems,* National Technical Information Service, Springfield, VA, 1984.

Namioka, T., "Theory of the Concave Grating. I" *Journal of the Optical Society of America,* vol. 49, p. 446, May 1959.

Roesler, F.L., "Fabry-Perot Instruments for Astronomy," *Methods of Experimental Physics, vol. 12, Part A: Optical and Infared,* Academic Press: New York, 1974.

Samson, J.A.R., *Techniques of Ultraviolet Spectroscopy,* John Wiley & Sons: New York, 1967.

INITIAL DISTRIBUTION LIST

1.	Defense Technical Information Center Cameron Station Alexandria, VA 22304-6145	2
2.	Library, Code 52 Naval Postgraduate School Monterey, CA 93943-5002	2
3.	Professor K.E. Woehler, Code PH Naval Postgraduate School Monterey, CA 93943	1
4.	Professor David Cleary, Code PH/Cl Naval Postgraduate School Monterey, CA 93943	3
5.	Professor Scott Davis, Code PH/Dv Naval Postgraduate School Monterey, CA 93943	1
6.	MAJ James W. Nichols 2786 Carlisle Rd. York, PA 17404	2
7.	Dr. Larry Paxton Johns Hopkins University Applied Physics Lab Johns Hopkins Rd. Laurel, MD 20723-6099	1